

# Magnetic properties of marine magnetotactic bacteria in a seasonally stratified coastal pond (Salt Pond, MA, USA)

Bruce M. Moskowitz,<sup>1</sup> Dennis A. Bazylinski,<sup>2</sup> Ramon Egli,<sup>3</sup> Richard B. Frankel<sup>4</sup> and Katrina J. Edwards<sup>5</sup>

<sup>1</sup>*Institute for Rock Magnetism, Department of Geology and Geophysics, University of Minnesota-Twin Cities, 310 Pillsbury Dr, SE, Minneapolis, MN 55455, USA. E-mail: bmosk@umn.edu*

<sup>2</sup>*School of Life Sciences, University of Nevada-Las Vegas, Las Vegas, NV 89154-4004, USA*

<sup>3</sup>*Department of Earth and Environmental Sciences, Ludwig-Maximilians-University, Theresienstr. 41, 80333 Muenchen, Germany*

<sup>4</sup>*Department of Physics, California Polytechnic State University, San Luis Obispo, CA 93407, USA*

<sup>5</sup>*Geomicrobiology Group, Department of Biological Sciences, University of Southern California, 316 Trousale Parkway, Los Angeles, CA 90089-0371, USA*

Accepted 2008 March 10. Received 2008 January 11; in original form 2007 August 6

## SUMMARY

Magnetic properties of suspended material in the water columns of freshwater and marine environments provide snapshots of magnetic biomineralization that have yet to be affected by the eventual time-integration and early diagenetic effects that occur after sediment deposition. Here, we report on the magnetism, geochemistry and geobiology of uncultured magnetite- and greigite-producing magnetotactic bacteria (MB) and magnetically responsive protists (MRP) in Salt Pond (Falmouth, MA, USA), a small coastal, marine basin (~5 m deep) that becomes chemically stratified during the summer months. At this time, strong inverse O<sub>2</sub> and H<sub>2</sub>S concentration gradients form in the water column and a well-defined oxic–anoxic interface (OAI) is established at a water depth of about 3.5 m. At least four morphological types of MB, both magnetite and greigite producers, and several species of magnetically responsive protists are found associated with the OAI and the lower sulphidic hypolimnion. Magnetic properties of filtered water were determined through the water column across the OAI and were consistent with the occurrence of magnetite- and greigite-producing MB at different depths. Sharp peaks in anhysteretic remanent magnetization (ARM) and saturation isothermal remanent magnetization (SIRM) and single-domain (SD) values of ARM/SIRM occur within the OAI corresponding to high concentrations of MB and MRP with magnetically derived cell densities of 10<sup>4</sup>–10<sup>6</sup> ml<sup>-1</sup>. Low-temperature (<300 K) remanence indicated that while only magnetite producers inhabit the OAI, both magnetite and greigite producers inhabit the sulphidic hypolimnion below the OAI. Magnetic measurements also show that the amount of Fe sequestered in magnetite magnetosomes within the OAI is no more than 3.3 per cent of the total available dissolved Fe(II) in the water column. However, below the OAI, magnetic minerals constitute a much larger fraction of the total dissolved Fe(II) ranging from 13.6 to 32.2 per cent depending on magnetic mineralogy. Most of this iron is possibly in the form of nanophase magnetic particles, possibly associated with biologically induced mineralization processes occurring below the OAI. Still, the OAI is a narrow but intense zone of SD particle production. Despite using just a small fraction of available dissolved Fe(II) in the water column for magnetosome production, the total number of MB living within an OAI, such as at Salt Pond, is all that is needed to produce the biogenic SD concentrations observed in some sediments. We also observed that Verwey transition temperatures fell within a narrow range of values between 95 and 105 K that were independent of both water depth and geochemical conditions. Reduced Verwey transition temperatures ( $T_v < 120$  K) appear to be an intrinsic property of magnetite magnetosomes whether grown in pure laboratory cultures or from a diverse population of magnetite-producing MB in the environment. This indicates that a limited amount of oxygen non-stoichiometry (>1 per cent) is present within magnetite magnetosomes, produced either

initially during magnetosome formation or subsequently as an 'aging' process in living magnetite-producing MB. Therefore, reduced values of the Verwey transition in biogenic SD magnetite in sediments do not necessarily indicate diagenetic alteration.

**Key words:** Biogenic magnetic minerals; Environmental magnetism; Rock and mineral magnetism.

## 1 INTRODUCTION

Since the discovery of magnetotactic bacteria (MB) by Blakemore (1975), these microorganisms and the iron mineral particles they biomineralize have been found in various aquatic environments that include marine sediments (e.g. Petersen *et al.* 1986; Vali *et al.* 1989; McNeill 1990; Petermann & Bleil 1993; Hesse 1994; Housen & Moskowitz 2006), lake sediments (e.g. Petersen *et al.* 1989; Peck & King 1996; Snowball *et al.* 2002; Pan *et al.* 2005a), chemically stratified marine and freshwater lakes and ponds (e.g. Bazylinski & Moskowitz 1997; Bazylinski *et al.* 2000; Simmons *et al.* 2004; Kim *et al.* 2005; Simmons & Edwards 2006) and some soils (Fassbinder *et al.* 1990). Diverse MB thrive in chemically stratified environments, mainly in proximity to the oxic–anoxic interface (OAI) (Bazylinski & Moskowitz 1997; Bazylinski *et al.* 2000; Simmons *et al.* 2004; Simmons & Edwards 2006). These bacteria synthesize magnetosomes, which are intracellular, membrane-bounded, single-magnetic-domain (SD) crystals of magnetite (Fe<sub>3</sub>O<sub>4</sub>) or greigite (Fe<sub>3</sub>S<sub>4</sub>) that are often arranged in single or multiple chains within the cell (Bazylinski & Frankel 2003). Magnetite- and greigite-producing magnetotactic bacteria (MMB and GMB, respectively) exert genetic control over the chemical composition, size, shape and crystallographic orientation of the magnetosomes as well as the chain architectures (e.g. Bazylinski & Frankel 2003; Komeili *et al.* 2006; Scheffel *et al.* 2006), trademarks of a biologically controlled mineralization (BCM) process. The chemical purity and the narrow size distribution of magnetite magnetosomes are reflected in their magnetic properties (Moskowitz *et al.* 1988, 1993; Weiss *et al.* 2004; Pan *et al.* 2005b; Kopp *et al.* 2006a,b; Pósfai *et al.* 2006a,b). Except for a few studies on single cells of GMB, the magnetic properties of greigite magnetosomes are poorly known because no GMB have yet been isolated and grown in pure culture (Penninga *et al.* 1995; Kasama *et al.* 2006; Pósfai *et al.* 2006b). Besides MB, magnetically responsive protists (MRP) containing magnetosome-like particles usually arranged in chains, have been identified in some chemically stratified marine environments (Bazylinski *et al.* 2000; Torres de Araujo *et al.* 1985). However, the magnetic properties of MRP are even more poorly characterized than the GMB.

In some freshwater and marine sediments, fossil magnetosomes or magnetofossils can typically account for 20–60 per cent of the bulk magnetization (Egli 2004a; Kim *et al.* 2005; Housen & Moskowitz 2006) and contribute to the paleorecords of geomagnetic field behaviour or to magnetic proxy records of paleoenvironmental changes (Chang & Kirschvink 1989; Hesse 1994; Snowball *et al.* 2002; Egli 2004a,b). In some situations, magnetofossils evidently survive diagenetic processes and have been found in 50 Ma deep sea sediments (Petersen *et al.* 1986), and possibly even in ancient consolidated sediments up to 2 billion years old (Chang *et al.* 1989; Kopp & Kirschvink 2007). Even more controversial is the debate on the origins of putative magnetite magnetofossils in carbonate inclusions in the 4.5 billion year old meteorite from Mars, ALH-84001 (Thomas-Keprta *et al.* 2000).

The identification and concentration of magnetosomes in sediments are usually inferred by electron microscopy and bulk mag-

netic measurements (Vali *et al.* 1989; Paasche *et al.* 2004; Weiss *et al.* 2004; Kim *et al.* 2005; Housen & Moskowitz 2006; Kopp *et al.* 2006a; Kopp & Kirshvink 2007). Strictly quantitative models for estimating the concentration of the magnetosomes with magnetic methods have been developed as well (Moskowitz *et al.* 1993; Egli 2004a,b; Weiss *et al.* 2004; Kopp *et al.* 2006a,b). The concentration of magnetosomes in sediments is controlled by the complex interaction between MB growth, sedimentation, geochemistry and early diagenesis (Canfield & Berner 1987; Leslie *et al.* 1990; Simmons & Edwards 2006). As a result, vertical profiles of magnetosome concentration are influenced by (1) the position of the OAI, often called the active oxidation front if it is located in the sediment (Bazylinski & Moskowitz 1997; Simmons *et al.* 2004), (2) environmental changes, such as those induced by anthropogenic activities (Hawthorne & McKenzie 1993; Egli 2004b) or climatic changes (Hesse 1994; Snowball *et al.* 2002; Pasche *et al.* 2004) and (3) sedimentary processes, such as early diagenesis (Leslie *et al.* 1990). The dominant morphology of magnetosomes (i.e. equant versus elongated) has been shown to be correlated with environmental parameters such as organic carbon influx (Yamazaki & Kawahata 1998), redox conditions (Egli 2004b) and paleoclimatic conditions (Hesse 1994). However, the reasons for these environmental chemistry correlations are unclear.

Magnetic properties of sediments are also affected by the activity of dissimilatory iron-reducing bacteria, which induce the extracellular precipitation of nanophase iron oxides including magnetite (e.g. Frankel & Bazylinski 2003; Banerjee 2006). This process is referred to as biologically induced mineralization (BIM). Unlike products of BCM, BIM products have a broad distribution of grain sizes and shapes, resulting in magnetic properties that are not particularly distinctive of its biological origins (Moskowitz *et al.* 1988, 1993; Bazylinski & Moskowitz 1997). Consequently the occurrence of BIM in sediments is not well constrained. In laboratory cultures, the dissimilatory iron reducer *Geobacter metallireducens* is capable of producing some 5000 times more magnetite than an equivalent biomass of MMB (Frankel 1987), but most of the nanophase magnetite is superparamagnetic (SPM) (<30 nm) at room temperature (Moskowitz *et al.* 1989). On the other hand, BIM magnetite is expected to undergo reductive dissolution much faster than magnetosomes because of its smaller grain size. Low-temperature magnetic measurements of marine and freshwater sediments suggest that significant amounts of nanophase magnetite are present (Tarduno 1995; Gibbs-Eggar *et al.* 1999; Smirnov & Tarduno 2000).

Chemically stratified marine and freshwater environments provide information about the occurrence, distribution, and geobiology of MB and dissimilatory iron-reducing bacteria, and the subsequent biogeochemical cycling of iron by these organisms (Bazylinski & Moskowitz 1997; Bazylinski *et al.* 2000; Simmons *et al.* 2004; Kim *et al.* 2005; Simmons & Edwards 2006). The integration of microorganism distributions over time and depth corresponds to the flux of BIM and BCM magnetic minerals into the sediment, before the occurrence of any diagenetic processes. The investigation of chemically stratified environments is, therefore, a first step in

understanding authigenic processes in sediments. We report here a detailed magnetic study of Salt Pond (Falmouth, MA, USA), a chemically stratified coastal pond containing diverse populations of MMB, GMB and MRP (Bazylinski & Moskowitz 1997; Bazylinski *et al.* 2000; Simmons *et al.* 2004).

## 2 SAMPLING AND EXPERIMENTAL METHODS

### 2.1 Sample site and sampling

Salt Pond is a small, seasonally chemically stratified marine basin located in Falmouth, MA ( $41^{\circ}32.6'N$ ,  $70^{\circ}37.7'W$ ) on the northeastern coast of the United States (Fig. 1). The pond is approximately 5.5 m deep with a surface area of  $0.26 \text{ km}^2$ . It has both marine and freshwater input and is connected to Vineyard Sound by a small inlet in the southwest corner of the pond (Giblin 1990; Bazylinski *et al.* 2000; Simmons *et al.* 2004). Salt Pond becomes stratified in early summer when hydrogen sulphide, produced by sulphate-reducing bacteria in the anaerobic zone and sediment, diffuses upwards while oxygen diffuses downwards from the surface. This results in a double, vertical chemical concentration gradient with a coexisting redox gradient. A strong pycnocline and other physical factors, probably including the microorganisms themselves, stabilize the vertical chemical gradients and the resulting OAI. During the summer, the sulphidic hypolimnion rises to within 3–4 m of the pond surface and the OAI becomes well defined near 3.5 m depth. Salt Pond was sampled in the early summer on 1996 July 07 and 1997 July 10, when the pond was stratified. Water samples were collected approximately every 0.1 m between 2.5 and 4.5 m water depths near the centre of the pond using a peristaltic pump (Fig. 1). Water was stored in 2-l plastic bottles and brought back to the lab within 4 hr after sampling. Water temperatures were close to the ambient air temperature so samples did not have to be kept cold but were kept in the dark.

### 2.2 Chemical analyses

Oxygen concentration profiles in the water column were obtained with an electronic oxygen sensor array that was lowered from a stable moored platform with a high-resolution winch. All dissolved

oxygen values were corrected for salinity and temperature. Water samples for sulphide and iron measurements were collected in line by syringe as described in Bazylinski *et al.* (2000) to prevent oxidation. Sulphide measurements were determined spectrophotometrically by the method of Cline (1969). Concentrations of iron species were determined by the use of the colorimetric reagent ferrozine as generally outlined by Lovley & Phillips (1987) and modified as described by Bazylinski *et al.* (2000).

### 2.3 Collection of magnetotactic bacteria

MB were collected from sample water bottles by placing the south pole of a bar magnet adjacent to the jar about 5–8 cm from the bottom and cell type identification were made from enrichment cultures. Water samples were examined for MB and MRP using a hanging drop technique in which a drop of water is suspended from the bottom of glass cover slip seated on an O-ring on a microscope slide, and phase-contrast light microscopy (Frankel *et al.* 1997). The organism inventory was determined for water depths between 3.0 and 4.2 m in 1996 and between 3.4 and 4.0 m in 1997.

### 2.4 Rock-magnetic measurements

Samples for magnetic measurements were prepared by filtering 100–200 ml of each of the water samples collected from discrete depths through  $0.22\text{-}\mu\text{m}$  filters (45 mm diameter, MEMBRA-FIL, Costar Corp., Cambridge, MA), which concentrated the suspended particulate matter composed of detrital minerals, organic matter particles and microorganisms. Unfortunately, while the  $0.22\text{-}\mu\text{m}$  filters are sufficient to collect MB cells, the retention of nanophase iron oxides on the filter is not ensured unless these particles are mechanically or chemically bound to larger grains or to microorganisms. A single filter was prepared for each depth. Filters were dried in air overnight, then folded into gelatin capsules and stored in a freezer prior to magnetic measurements. All room temperature magnetic measurements (ARM, SIRM, hysteresis loops) reported here were completed within 2 weeks from the time water samples were initially collected at Salt Pond to minimize aging effects. Low-temperature measurements took an additional 2–4 weeks to complete.

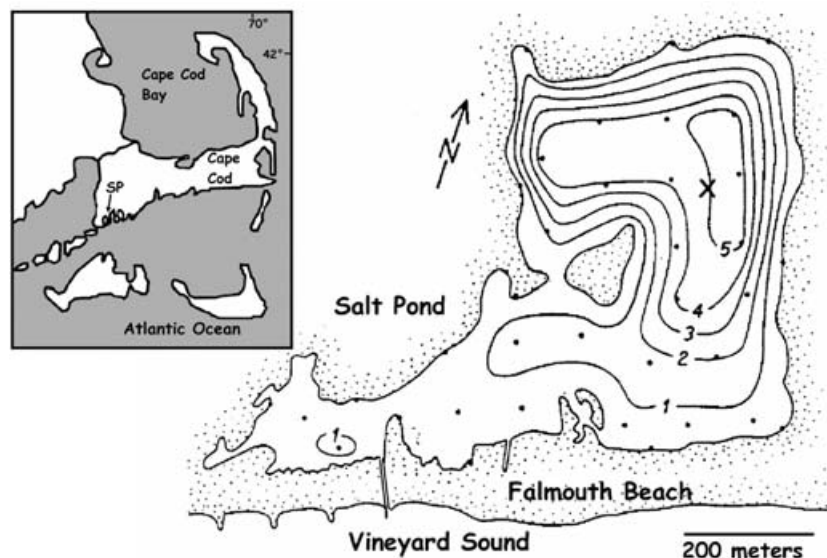


**Figure 1.** Site location map and bathymetry for Salt Pond (SP), Cape Cod, Massachusetts. Bathymetric contours are in meters. X indicates water-sampling location in 1996 and 1997. [adapted from Giblin (1990) and Simmons *et al.* (2004)].

Magnetization values are given as magnetic moment per volume of water filtered ( $A\ m^2\ l^{-1}$ ).

Saturation isothermal remanent magnetization (SIRM) and anhysteretic remanent magnetization (ARM) were measured using a SQUID rock magnetometer (2G Corp. SRM model 760-R). ARM was acquired in a dc field of  $50\ \mu T$  and peak ac field of  $100\ mT$ . SIRM was produced in a saturating field of  $1.0\ T$  using a pulse magnetizer. Low-temperature remanence ( $20\text{--}300\ K$ ) was measured with a Quantum Design (MPMS2) SQUID magnetometer. Saturation remanence acquired in a  $2.5\ T$  field at  $20\ K$  was measured on warming from  $20$  to  $300\ K$  following two different magnetic field protocols: (1) cooling samples down from  $300$  to  $20\ K$  in a zero magnetic field (zero field cooled, ZFC) and (2) cooling samples to  $20\ K$  in a  $2.5\ T$  field (field cooled, FC).

The FC–ZFC protocol can be used to identify SD magnetite based on the difference between FC and ZFC magnetizations upon warming through the Verwey transition in magnetite, which for stoichiometric magnetite occurs at  $T = 120\ K$  (Moskowitz *et al.* 1993). Delta–delta ratios ( $\delta_{FC}/\delta_{ZFC}$ ), defined as the ratio of the Verwey transition amplitude for the FC and ZFC treatments with  $\delta = (M_{80K} - M_{150K})/M_{80K}$  and  $M$ , the remanent magnetization at  $80$  or  $150\ K$ , were calculated from the SIRM measurements (Moskowitz *et al.* 1993). Delta–delta ratios greater than  $1.0$  are diagnostic of SD magnetite while ratios greater than  $2.0$  are characteristic of MMB that have magnetite magnetosomes organized in chains. Disruption of the chain structure, partial or complete magnetosome oxidation, or mixing with other magnetic phases (e.g. greigite) or SPM particles can reduce the delta–delta ratio below  $2.0$  (Moskowitz *et al.* 1993; Weiss *et al.* 2004; Housen & Moskowitz 2006; Kopp *et al.* 2006a,b). A model proposed by Carter-Stiglitz *et al.* (2002, 2004) interpreted the high values of  $\delta_{FC}/\delta_{ZFC} > 2.0$  as originating

from a combination of the positive magnetostatic interactions within chains of magnetosomes, field-induced easy-axis alignment below the Verwey transition, and minor amounts ( $<1$  per cent) of oxygen non-stoichiometry.

Hysteresis loops and the coercivity of remanence ( $H_{cr}$ ) were measured at room temperature with a vibrating sample magnetometer (Princeton Measurements) for the 1997 samples and with the MPMS2 for the 1996 samples. Coercivity of remanence was determined either from standard back-field measurements (1997 samples) or with the  $\Delta M$  method (1996 samples). The latter uses the difference between the ascending and descending branches of a hysteresis loop to estimate  $H_{cr}$  (Tauxe *et al.* 1996). Sample magnetization was too weak to measure AC susceptibility properties, detailed coercivity analysis of demagnetization curves or FORC diagrams.

### 3 RESULTS

#### 3.1 Water column chemistry

Chemical profiles in the water column for 1996 July 07 and 1997 July 10 are shown in Fig. 2. There is an inverse double concentration gradient of oxygen diffusing downwards from the surface and sulphide generated by sulphate-reducing bacteria in the anaerobic zone diffusing upwards. On 1996 July 09, the OAI extended from about  $3.3\ m$ , where oxygen became undetectable, to  $3.5\ m$ , where hydrogen sulphide first became detectable at  $>1\ \mu M$  (Fig. 2a). By  $3.6\ m$ , the sulphide concentration was greater than  $100\ \mu M$ . On 1997 July 10, the OAI was slightly wider extending from  $3.1$  and  $3.5\ m$ . The sulphide concentration was greater than  $100\ \mu M$  by  $3.7\ m$  and increased to near  $1\ mM \times 4.0\ m$  (Fig. 2b). In 1996, sulphide concentrations were only determined to a

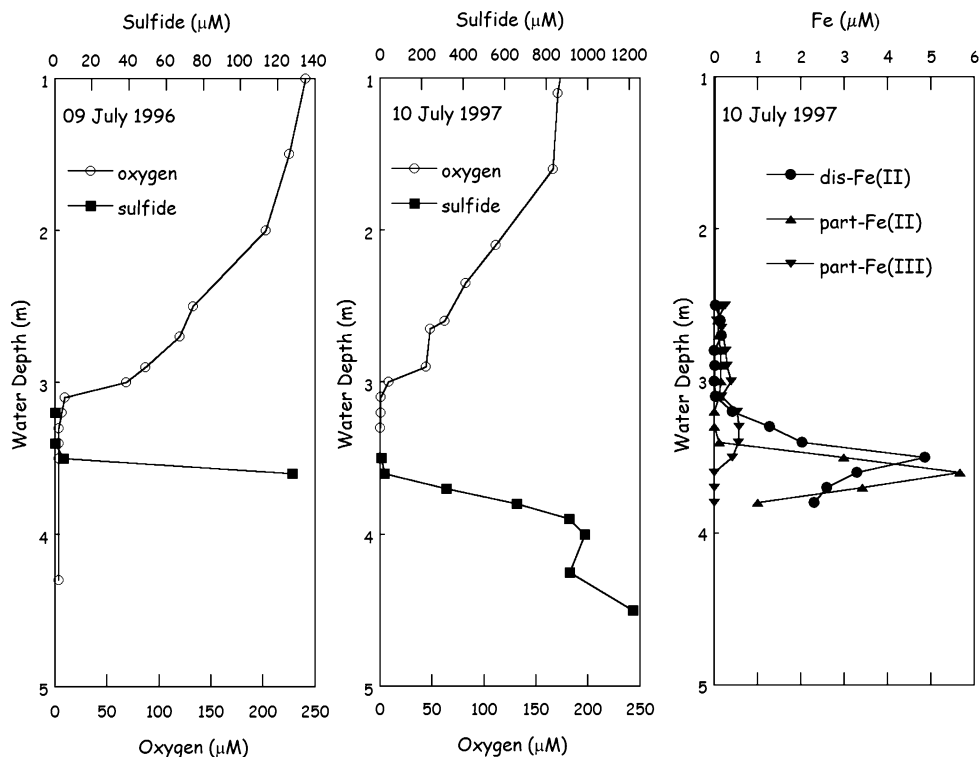


**Figure 2.** Chemical profiles of dissolved oxygen and sulphide in the water column from Salt Pond sampled on (a) 1996 July 9 and (b) 1997 July 10. (c) Dissolved and particulate iron concentrations for 1997 July 10. In 1996, sampling for sulphide was limited to a maximum depth of  $3.6\ m$ , where sulphide concentrations just begin to increase to high levels.

maximum water depth of 3.6 m in order to locate the base of the OAI. At deeper depths, sulphide concentrations are presumed to have been similar to those observed in 1997. Total dissolved and particulate Fe concentrations for 1997 were a maximum at the base of the OAI (Fig. 2c).

### 3.2 Magnetotactic bacteria and protists

Microscopic observations show that there were at least four morphological types of MB, two MMB (cocci and short rods) and two GMB (long rods and the many-cell magnetotactic prokaryote (MMP), now called *Candidatus Magnetoglobus multicellularis*; Abreu *et al.* 2007), associated with the OAI and the sulphidic zone below it, respectively (see also Simmons *et al.* 2004). MMB existed in greatest number within the OAI where microaerobic conditions predominated, while GMB were found at the bottom of, or below, the OAI where sulphide concentration became detectable.

Magnetosome arrangements vary from simple linear chain configurations to more complex configurations (Fig. 3). The short rod MMB produce a single linear chain of magnetosomes whereas the cocci MMB do not (Figs 3a and b). Cocci with magnetosomes not arranged in chains have been reported elsewhere (Towe & Moench 1981; Pósfai *et al.* 2006b). The magnetosomes in the cocci are clearly elongated, and there is a consensus alignment of the long

axes of the magnetite crystals. It is unlikely that the non-chain arrangement in the cocci (and in the GMB in Figs 3c and d) is due to grid preparation, which consists of placing cells on the grid in a drop of water and drying. This may cause the cell to break (especially if the grid is washed with distilled water after cell deposition), but if the cell remains intact, it is difficult to explain how the magnetosomes would rearrange themselves as in Fig. 3(a), that is, with relatively parallel long axes and uniform spacings.

In addition to MB, several different MRP, including two types of biflagellates, a dinoflagellate, and a ciliate (*Cyclidium* sp.), were also present (Bazylinski *et al.* 2000). Magnetic particles in the biflagellates and the dinoflagellate were identified as magnetite, while those in the ciliate have unknown composition (Bazylinski *et al.* 2000). The morphological types and cell densities of the protists, like those of the MB, were also dependent on water depth. Examples of the different types of magnetic microorganisms are shown in Figs 3 and 4, and the cell inventory is given in Table 1.

### 3.3 Mineral magnetic profiles

#### 3.3.1 Concentration and grain size indicators

Concentration dependent properties (ARM, SIRM and  $M_s$ ) of the filtrates as a function of water depth are shown in Fig. 5 (1996) and Fig. 6 (1997). ARM intensity (Figs 5a and 6a) for both sampling years show peaks in magnetic remanence near or within the OAI

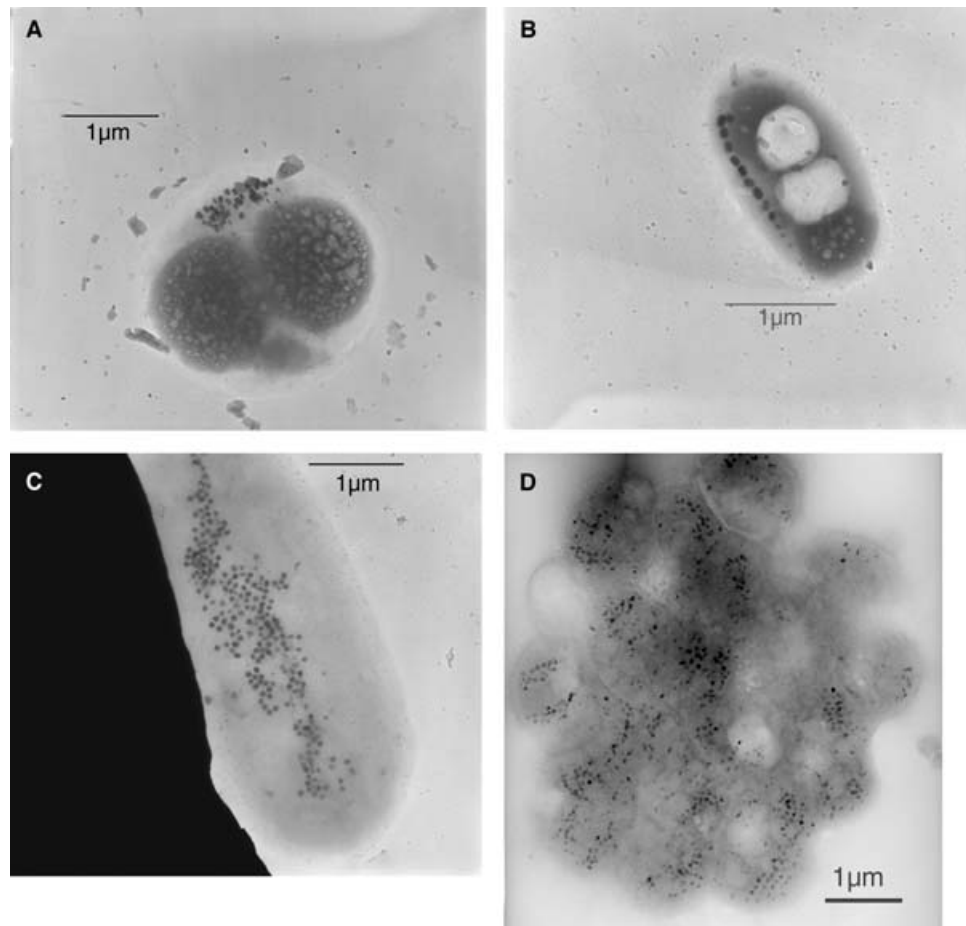


**Figure 3.** Transmission electron micrographs of the four dominant prokaryotes found at Salt Pond on 1997 July 10: (a) a magnetotactic coccus with magnetite magnetosomes; (b) a small magnetotactic rod with magnetite magnetosomes; (c) a large magnetotactic rod with greigite magnetosomes and (d) a multicellular, magnetotactic prokaryote (MMP) with greigite magnetosomes (*Candidatus Magnetoglobus multicellularis*).

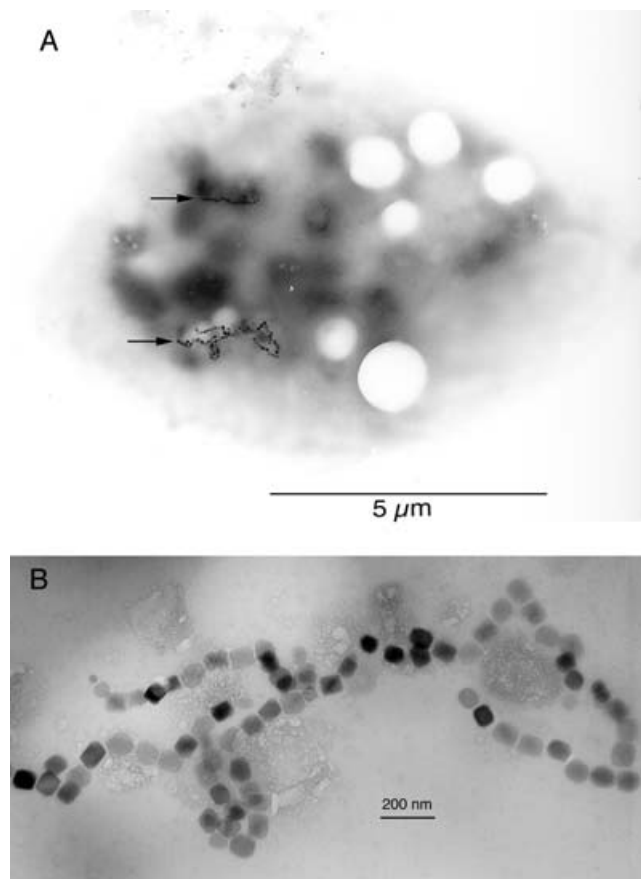


**Figure 4.** Transmission electron micrograph of Biflagellate 'c' (Bazylinski *et al.* 2000), a magnetically responsive protist (MRP) found below the OAI at Salt Pond on 1997 July 10. The arrows indicate chains of putative magnetosomes in the cell. (b) An enlarged view of the magnetosomes at the lower part of the image shown in (a). The magnetosome crystals were identified as magnetite by selected area electron diffraction (M. Pósfai, private communication, 2003).

and corresponded to the location where MB were observed to occur in great numbers. The 1996 profile (Fig. 5a) showed a sharp increase in ARM intensity just above the OAI at 3.2 m followed by a broad maximum extending through the OAI. Peak ARM intensity was  $40 \text{ nA m}^2 \text{ l}^{-1}$ . At the base of the OAI, ARM intensities decreased gradually with depth over the interval between 3.6 and 4.5 m. In contrast, the 1997 profile (Fig. 6a) showed a gradual increase in ARM intensity within the OAI raising to a sharp peak at the bottom of the OAI at 3.5 m. The 1997 peak ARM intensity was  $160 \text{ nA m}^2 \text{ l}^{-1}$ , which was nearly a fourfold increase in peak ARM intensity over the previous year. However, ARM intensities at depths just 0.1 m away from the peak 1997 value at 3.5 m were comparable to those from 1996.

SIRM intensity depth profiles are shown in Fig. 5(b) (1996) and Fig. 6(b) (1997). The shapes of the SIRM depth profiles were similar to the ARM profiles for each year. Peak SIRM intensities also showed the nearly fourfold increase between 1996 ( $300 \text{ nA m}^2 \text{ l}^{-1}$ ) and 1997 ( $1200 \text{ nA m}^2 \text{ l}^{-1}$ ) as observed with the ARM data. However, unlike the ARM profiles, SIRM intensities at depths below the 1997 peak at 3.5 m stayed significantly higher ( $>2x$ ) than the 1996 SIRM values.

Saturation magnetization ( $M_s$ ) depth profiles are shown in Fig. 5(c) (1996) and Fig. 6(c) (1997). The  $M_s$  profiles were sim-

**Table 1.** Cell inventory as a function of water depth in Salt Pond.

Depth (m)	1996 July 09	1997 July 10
3.0	MRP(a)	nd
3.1	MRP(b)	nd
3.2	MMB(cocci*)	nd
3.3	MRP(a)	
	MMB (short rod*)	nd
	MRP(b)	
3.4	nd	MRP (b*)
		MMB(short rod*, cocci)
3.5	nd	MRP(a, c*, d*)
		MMB (short rod, cocci),
		GMB (MMP)
3.6	MMB (short rod, cocci.)	GMB (MMP*, large rod)
	MRP (c)	MRP (c*, d, a)
		MMB (cocci)
3.7	MMP, large rod, short rod	GMB (large rod*, MMP),
	MRP (c*)	MRP (c)
3.8	GMB (MMP, large rod)	GMB (MMP, large rod)
	MRP(c,d)	MRP(c)
3.9	nd	Fewer organisms than at 3.8m
		GMB (MMP)
		MRP (c)
4.0	nd	Fewer organisms than at 3.9m
		GMB (MMP, large rod)
		MRP (c)
4.2	GMB (MMP, large rod)	nd
	MRP (c)	

*Notes:* MRP, magnetically responsive protist; MMB, magnetite-producing magnetotactic bacteria; GMB, greigite-producing magnetotactic bacteria; MMP, *Candidatus Magnetoglobus multicellularis*. MRP includes Dinoflagellate 'a', Biflagellate 'b', Biflagellate 'c' and Ciliate 'd' (*Cyclidium* sp.) (Bazylinski *et al.* 2000). \* indicates a microorganism that occurred in very high numbers compared to others at a particular depth based on phase-contrast light microscopy. nd indicates depths where the cell inventory was not determined.

ilar to the remanence profiles (ARM, SIRM), but with some notable differences below the OAI. In addition to a maximum in  $M_s$  associated with the OAI, there was a deeper zone where  $M_s$  was also elevated. The 1997 profile (Fig. 6c) showed two peaks in  $M_s$  at 3.5 and 4.0 m. The second peak at 4.0 m on the 1997 profile was actually higher than the peak associated with the zone where MB occurred in greatest number (3.5 m). Although there was a slight increase in SIRM and ARM also at this depth (Figs 6a and b), neither remanences at 4.0 m were anywhere near the peak ARM or SIRM values associated with the OAI. In 1996, instead of a second deeper  $M_s$  peak, the saturation magnetization profile (Fig. 5c) showed a slight but steady increase in  $M_s$  with depth starting at 4.1 m and continuing to the last depth sampled at 4.5 m.  $M_s$  values in 1997 were approximately five times larger than in 1996. This deeper zone of increasing  $M_s$  was not accompanied by a similar increase in ARM or SIRM intensities.

The SIRM at 20 K, after zero field cooling (ZFC-SIRM) and field cooling (FC-SIRM), as a function of water depth for both sampling dates is shown in Figs 5(d) and 6(d). The trends with water depth matched the variation found for room temperature ARM and SIRM. The largest offsets between ZFC and FC remanences, with FC-SIRM  $>$  ZFC-SIRM occurred within and below the OAI and were due to the magnetic effects associated with the Verwey transition (Moskowitz *et al.* 1993; Carter-Stiglitz *et al.* 2004; Muxworthy & Williams 2006). The deeper zones where  $M_s$  increased near, or

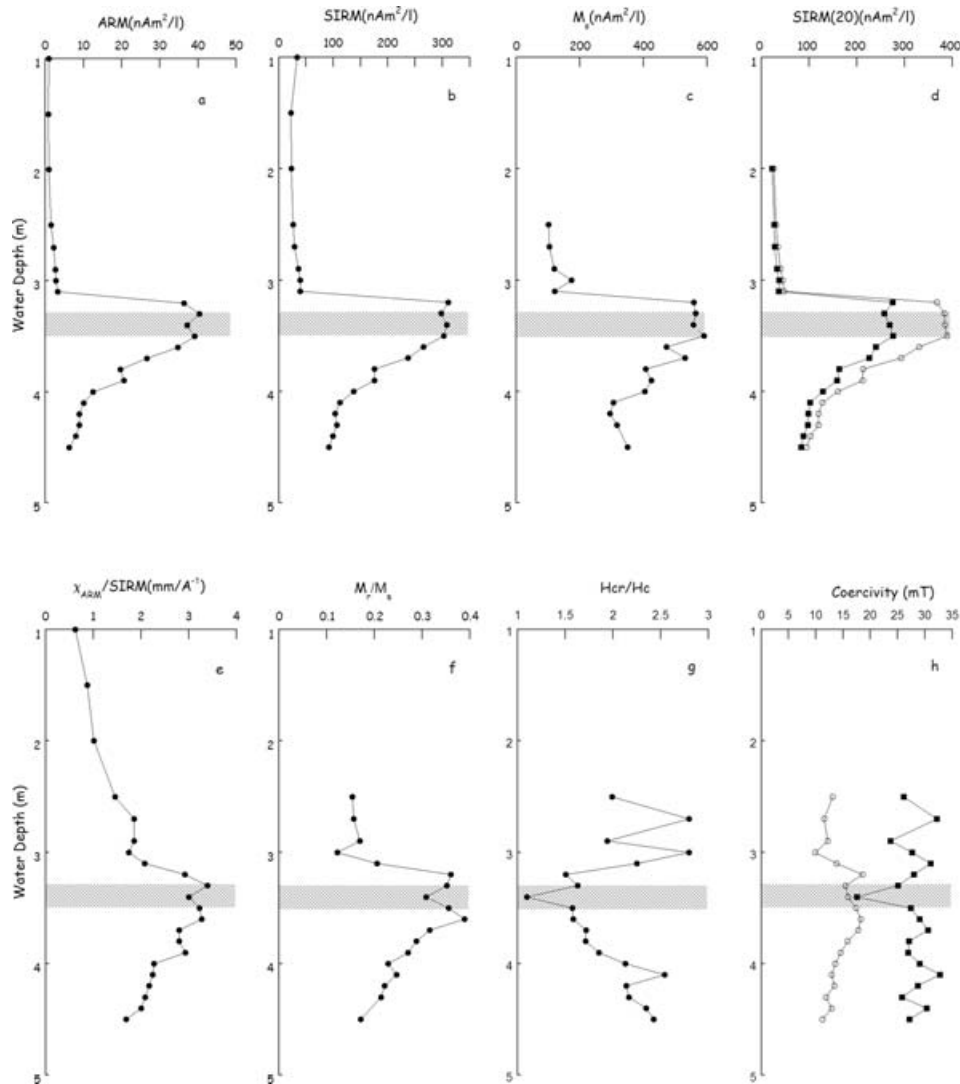


**Figure 5.** Mineral magnetic property profiles as a function of water depth for Salt Pond sampled on 1996 July 09. Hatched zone is the location of the OAI based on the chemical profiles in Fig. 2(a). Concentration dependent magnetic parameters include (a) ARM, (b) saturation remanence (SIRM), (c) saturation magnetization ( $M_s$ ) and (d) saturation remanence at 20 K after field cooling (open symbol, FCSIRM) and zero-field cooling (closed symbol, ZFCSIRM). Magnetic grain size indicators include (e) ARM ratio, ( $\chi_{\text{ARM}}/\text{SIRM}$ ), (f) remanence ratio ( $M_r/M_s$ ), (g) coercivity ratio ( $H_{\text{cr}}/H_c$ ) and (h) coercivity ( $H_c$ ) and coercivity of remanence ( $H_{\text{cr}}$ ).

below, 4 m (Figs 5c and 6c) corresponded to a depth interval where ZFCSIRM and FCSIRM are nearly constant.

Grain size indicators ( $\chi_{\text{ARM}}/\text{SIRM}$ ,  $M_r/M_s$ ) for the 1996 and 1997 profiles are shown in Figs 5(e), (f) and 6(e), (f), respectively. Similar depth trends in the  $\chi_{\text{ARM}}/\text{SIRM}$  ratio were observed for both years:  $\chi_{\text{ARM}}/\text{SIRM}$  values were  $< 2.0 \text{ mm A}^{-1}$  in the zone above 2.9 m, increasing to maximum values ( $\sim 3.0 \text{ mm A}^{-1}$ ) between 2.9 and 3.7 m, and then decreasing to values less than  $2.0 \text{ mm A}^{-1}$  again at depths below about 3.8 m. For the 1997 data set,  $\chi_{\text{ARM}}/\text{SIRM}$  showed a double maximum, with one occurring at 3.1 m, at the top of the OAI and the other at 3.5 m, at the bottom of the OAI. The second peak at 3.5 m matched the maximum in both ARM and SIRM intensities. The double maxima associated with the OAI were not as pronounced in the 1996 profile. The peak  $\chi_{\text{ARM}}/\text{SIRM}$  values within the OAI were similar to values observed for cultured MMB ( $\chi_{\text{ARM}}/\text{SIRM} = 2.5\text{--}3.5 \text{ mm A}^{-1}$ ; Moskowitz *et al.* 1988, 1993; Kopp *et al.* 2006a,b), and for magnetic components related to well preserved magnetofossils in marine and freshwater sediments ( $\chi_{\text{ARM}}/\text{SIRM} = 1.5\text{--}5.0$ ; Egli 2004a). Theoretical calculations pre-

dict  $\chi_{\text{ARM}}/\text{SIRM}$  is greater than  $2.0 \text{ mm A}^{-1}$  for non-interacting, SD magnetite particles similar to magnetosomes (Egli & Lowrie 2002).

Hysteresis parameters showed systematic variations with water depth (Figs 5f, g and 6f, g). SD-like values ( $M_r/M_s > 0.2$  and  $H_{\text{cr}}/H_c < 2.0$ ) occurred within the zones associated with high values of ARM, SIRM and  $\chi_{\text{ARM}}/\text{SIRM}$  and corresponded to depths within the OAI. Away from the OAI towards shallower or deeper water depths,  $M_r/M_s$  decreased and  $H_{\text{cr}}/H_c$  increased, indicating a significant fraction of either coarser grain MD particles ( $> 1000 \text{ nm}$ ), or nanophase SPM particles ( $< 30 \text{ nm}$ ). Additionally, non-chain or closely grouped magnetosome arrangements observed in some of the MMB, GMB and MRP (see Figs 3 and 4) could also reduce  $M_r/M_s$  ratios below the theoretical value for non-interacting SD particles.  $M_r/M_s$  ratios were systematically higher throughout the water column in 1996 than in 1997. Coercivities (Figs 5h and 6h) increased near the top of the OAI and then dropped either sharply (1997) or gradually (1996) below the OAI. Maximum values of coercivities were similar for both years with  $\mu_0 H_c \approx 18 \text{ mT}$  and

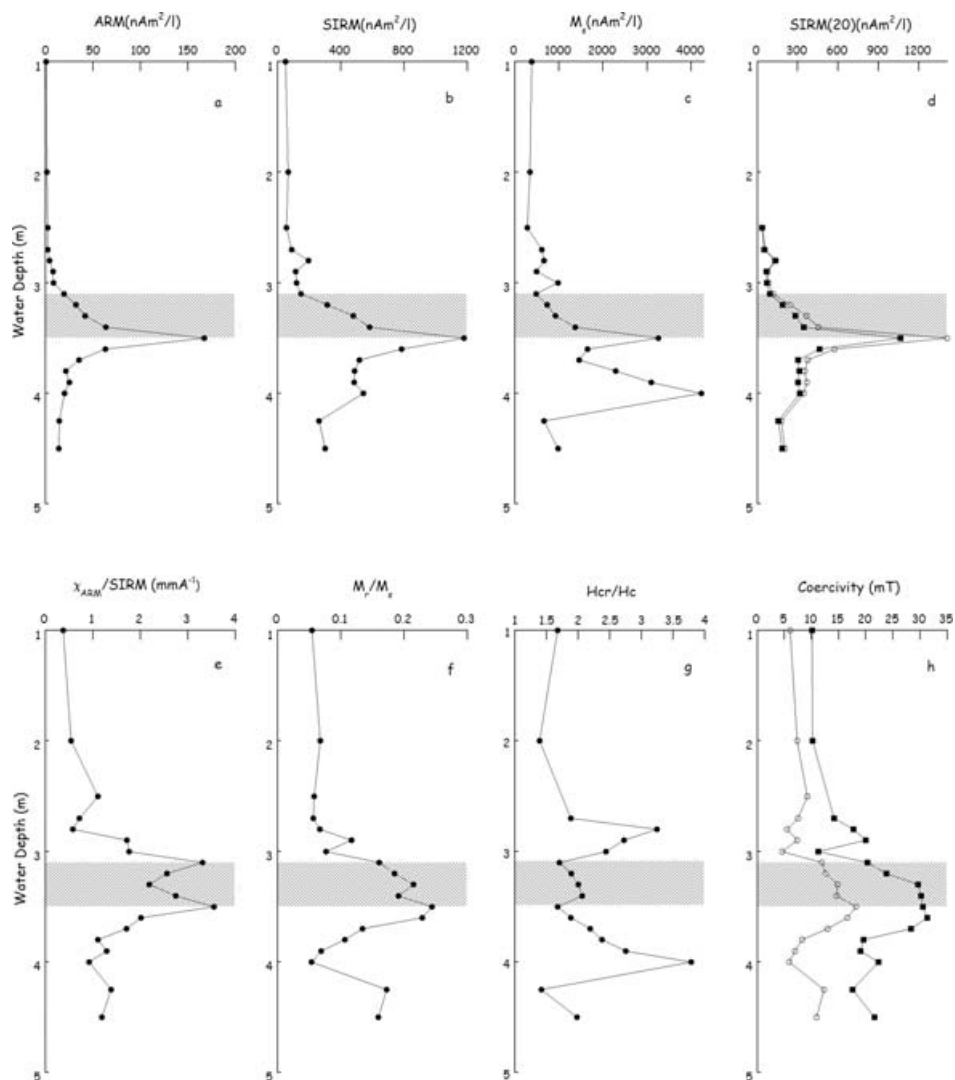


**Figure 6.** Mineral magnetic property profiles as a function of water depth for Salt Pond sampled on 1997 July 10. Hatched zone is the location of the OAI based on the chemical profiles in Fig. 2(b). Concentration dependent magnetic parameters include (a) ARM, (b) saturation remanence (SIRM), (c) saturation magnetization ( $M_s$ ) and (d) saturation remanence at 20 K after field cooling (open symbol, FCSIRM) and zero-field cooling (closed symbol, ZFCSIRM). Magnetic grain size indicators include (e) ARM ratio, ( $\chi_{ARM}/SIRM$ ), (f) remanence ratio ( $M_r/M_s$ ), (g) coercivity ratio ( $H_{cr}/H_c$ ) and (h) coercivity ( $H_c$ ) and coercivity of remanence ( $H_{cr}$ ).

$\mu_0 H_{cr} \approx 30$  mT, although the  $H_{cr}$  data for the 1996 profile showed considerably more scatter with depth. This was most likely the result of the overall weak magnetizations and from the  $\Delta M$  method of calculating  $H_{cr}$ , which required the subtraction of the ascending from the descending branches of the hysteresis loop, both of which were noisy. For both sampling dates, coercivities ( $H_c$  and  $H_{cr}$ ) were low compared to coercivity observed for cultured, single-chain MMB or from single cell MB measurements (Moskowitz *et al.* 1993; Penninga *et al.* 1995; Hanzlik *et al.* 2002; Weiss *et al.* 2004; Kopp *et al.* 2006a,b). Non-chain or closely grouped magnetosome arrangements could reduce coercivity values from those observed in single-chain MMB (Penninga *et al.* 1995).

### 3.3.2 Low-temperature magnetic properties

The variation in FCSIRM demagnetization curves with depth is shown in Fig. 7 (1996) and Fig. 8 (1997). At all depths, the Verwey transition was observed near  $T = 100$  K, consistent with the presence of magnetite. Distinctive remanence transitions associated

with pyrrhotite or siderite were not observed. Near surface samples ( $<2.5$  m in 1996 and  $<3.0$  m in 1997) displayed SPM-type demagnetization behaviour with a smeared-out magnetite transition. Starting at 3.2 m and extending down to 3.9 m, the Verwey transition became well developed for both sampling dates, indicating a predominance of MMB at these depths. Below 4.0 m, the Verwey transition amplitude again became weaker but never disappeared. Also below the OAI, the high-temperature slopes of the FCSIRM curves above the Verwey transition ( $T > 120$  K) became steeper indicating a possible SPM component with unblocking temperatures between 120 and 300 K. Verwey transition temperatures, estimated from the first derivative of the FCSIRM curves, were between 95 and 105 K and showed no systematic variation with water depth below 2.9 m.

Examples of FC and ZFC demagnetization curves at selective water depths are shown in Fig. 9. Nearly all samples showed bifurcated FC–ZFC curves below the Verwey transition with FC remanence greater than the ZFC remanence, indicating the presence of SD magnetite. Delta–delta ratio profiles for both summers

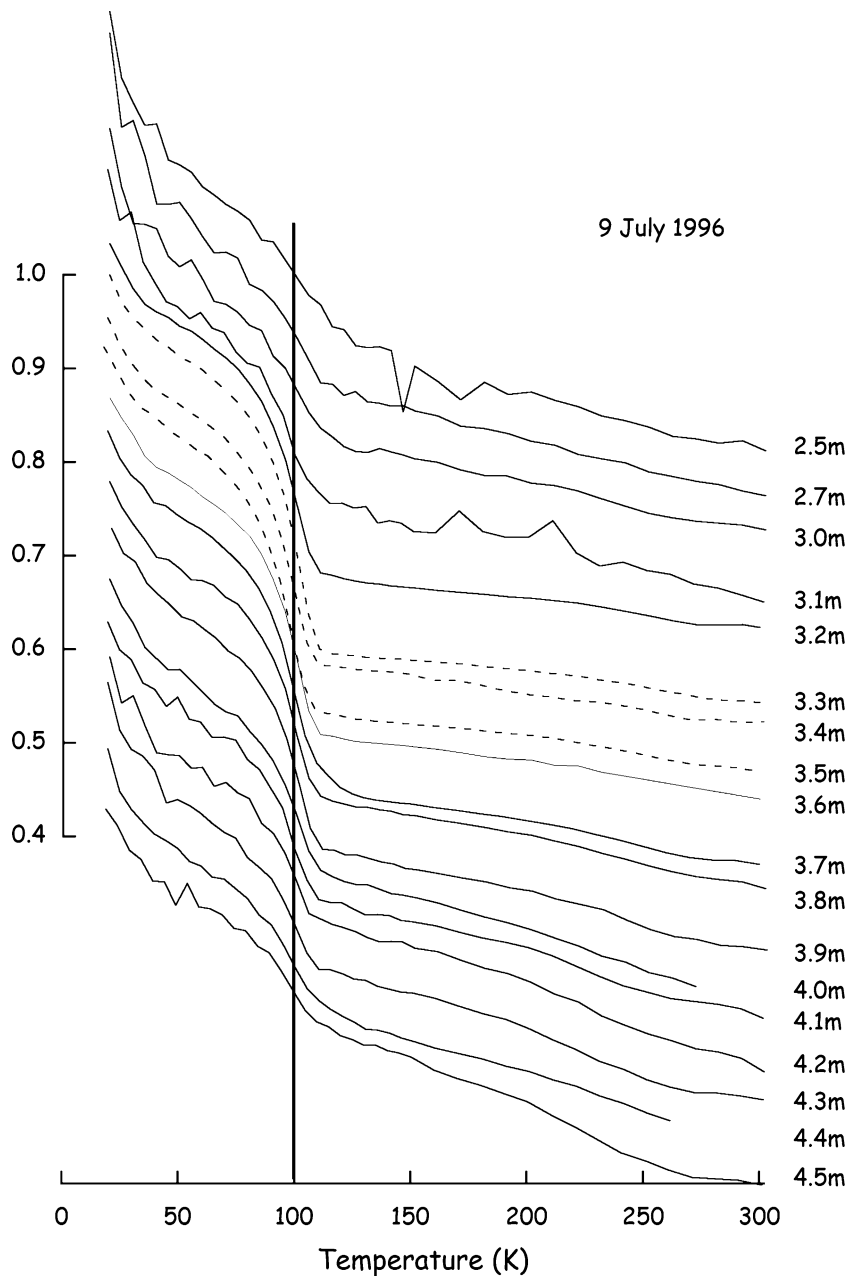


**Figure 7.** Normalized FCSIRM demagnetization curves as a function water depth for 1996 July 9. Each curve is normalized by its SIRM at 20 K and spans the same vertical scale as shown by the vertical axis. Curves are offset from each other for clarity and labelled on the right by water depth. The vertical line at 100 K represents an approximate upper bound to observed Verwey transition temperatures. Dashed curves represent samples from OAI. The FCSIRM demagnetization curves are shown instead of the ZFCSIRM curves because field cooling enhances the magnetic transitions associated with the Verwey transition in SD magnetite and allows for easier identification.

(Fig. 10) showed similar trends with delta–delta ratios exceeding 2.0 beginning at 3.0 m. For the 1996 profile, there were two peaks with the first peak at 3.3 m with  $\delta_{FC}/\delta_{ZFC} = 3.1$  and the second at 3.9 m with  $\delta_{FC}/\delta_{ZFC} = 2.6$ . The delta–delta ratio dropped back below 2.0 at 4.3 m. For the 1997 profile, the zone of elevated delta–delta ratios was confined to the OAI with peaks at 3.1 and 3.5 m with  $\delta_{FC}/\delta_{ZFC} \approx 2.5$ . The delta–delta ratio became less than 2.0 at 3.6 m.

### 3.3.3 Superparamagnetic particles

Any estimates of the SPM contribution will almost certainly be minimum values due to sampling bias because the 0.22- $\mu\text{m}$  filters will

under sample the SPM fraction unless the nanometre-sized particles were attached to larger particles or microorganisms that do not pass through the filters. Unfortunately, due to the very weak magnetizations of the filtrates, AC susceptibility could not be measured to assess the SPM contribution. As an alternative approach, the contributions from SPM particles were estimated from the high-temperature (120–220 K) slopes (HTS) of the ZFCSIRM demagnetization curves. It is assumed that any change in remanence with temperature from above the Verwey transition (120 K) to 220 K is due entirely to the thermal unblocking of SPM particles with blocking temperatures between 120 and 220 K. For a spherical particle of magnetite or greigite with a microcoercivity of 50 mT and blocking

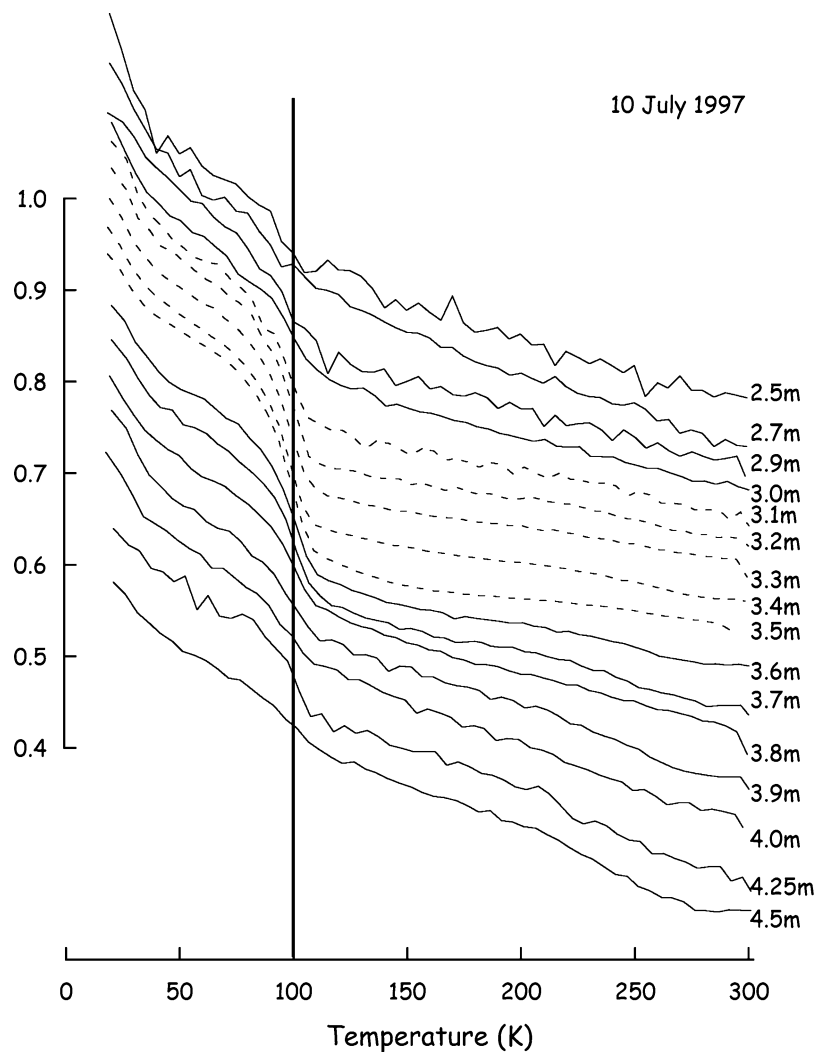


**Figure 8.** Normalized FCSIRM demagnetization curves as a function water depth for 1997 July 10. Each curve is normalized to its SIRM at 20 K and spans the same vertical scale as shown by the vertical axis. Curves are offset from each other for clarity and labelled on the right by the water depth. The vertical line at 100 K represents an approximate upper bound to observed Verwey transition temperatures. Dashed curves represent samples from OAI.

temperature of 120 K obeying Néel relaxation, this would correspond to a SPM particle with a diameter of 19 nm for magnetite or 29 nm for greigite. The effects due to the temperature dependence of  $M_s$  and of non-uniform magnetization states of large SD and small PSD particles are ignored. However, an estimate of the effect of the temperature dependence of  $M_s$  on HTS for magnetite magnetosomes can be obtained from the empirical law  $M_s(T) = (T_c - T)^\gamma$ , where  $T_c = 853$  K is the Curie temperature of magnetite and  $\gamma = 0.43$  is an empirical constant (Dunlop & Özdemir 1997). This calculation yields a concentration independent value of  $\text{HTS}/M_s(220 \text{ K}) = 0.00065 \text{ T}^{-1}$ , which will be identified as a minimum background value unrelated to unblocking of SPM particles.

HTS was determined from linear regression of the ZFSIRM curves and the results are presented in two ways: (1) normalized by volume ( $\text{ml}^{-1}$ ) representing a parameter related to the absolute concentration of SPM particles and (2) normalized by ZFSIRM at 220 K (MZFC) representing a concentration independent parameter (HTS/MZFC) related to relative variations in the amount of unblocked (SPM) to blocked (SD + MD) material. High (low) values of HTS/MZFC indicate more (less) SPM material relative to SD + MD component.

In 1996, the variation of SPM concentration with depth (Fig. 11a) showed a sudden increase at the top of the OAI and then remained fairly constant at this level down to the base of the section. Similarly in 1997, there was an increase in the SPM fraction at the top of the OAI, but unlike 1996 there was more fluctuation in the SPM concentration with depth below the OAI. During both years, the maximum SPM concentration occurred at the base of the OAI at 3.5 m. In terms of the HTS/MZFC ratio (Fig. 11b), similar trends were observed for both years. At the top of the OAI, HTS/MZFC decreased sharply and then remained at low values within the OAI where MB were most abundant. Beginning just below the base of the OAI, HTS/MZFC increased with depth. For comparison, the range in values for HTS/MZFC for several strains of MMB grown in pure culture (Moskowitz *et al.* 1993, unpublished data), along with the theoretical minimum background, are shown in Fig. 11(b). Low values of HTS/MZFC within the OAI match the values for cultured MMB and the theoretical estimate and indicate that this parameter tracks the SPM/SD ratio. The peaks in HTS and HTS/MZFC at 2.8 and 4.0 m in 1997 corresponded to the two high values in  $H_{cr}/H_c$  and low values in  $M_r/M_s$  (Fig. 6g) consistent with a mixture of SPM and SD particles. Mixtures of SPM and SD particles may help to

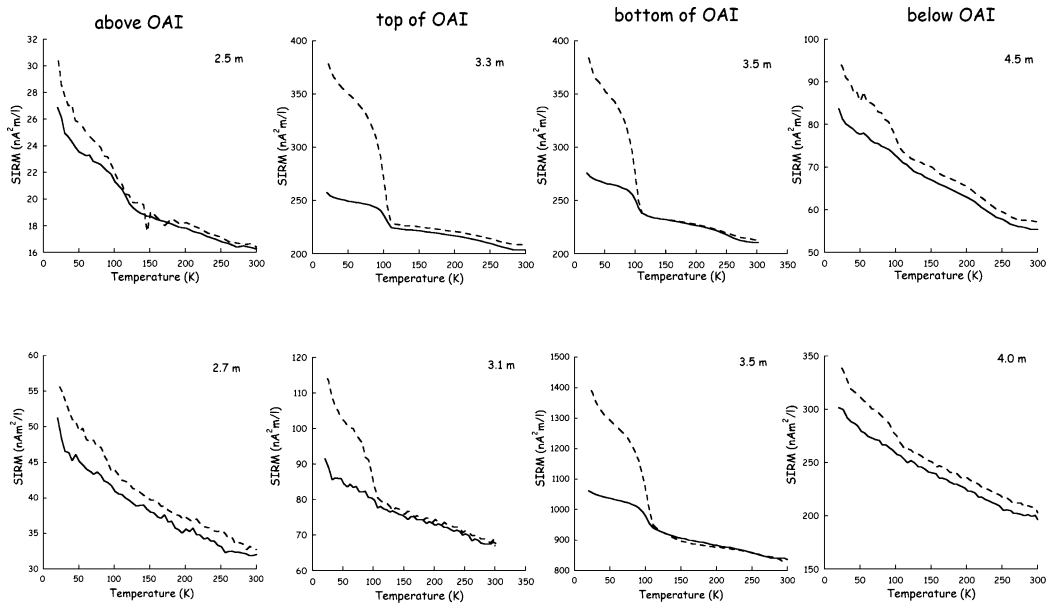


**Figure 9.** Low-temperature FC (dashed line) and ZFC (solid line) demagnetization curves for selected water depths corresponding to above the OAI, top of OAI, bottom of OAI, and below the OAI. Top row for data collected on 1996 July 09 and bottom row for data collected on 1997 July 10.

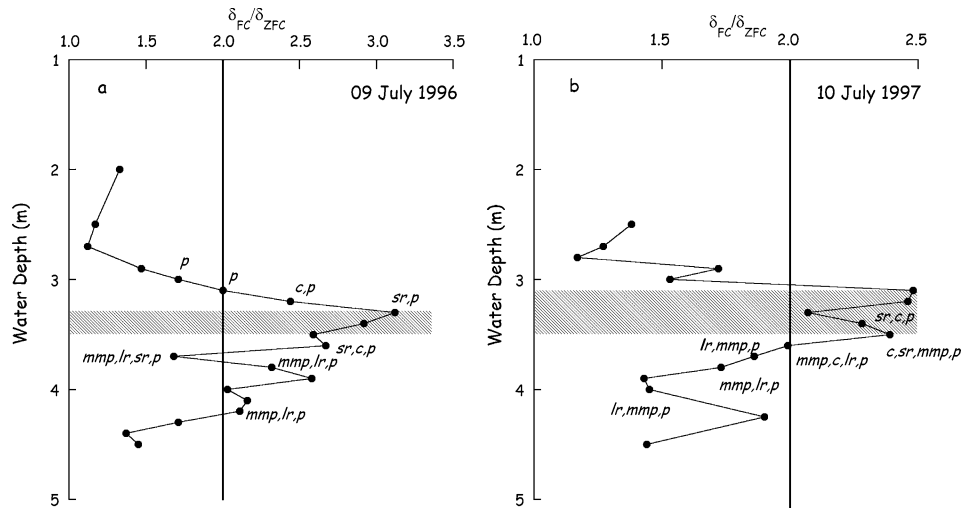


**Figure 10.** Delta-delta ratios as a function of water depth for samples collected on (a) 1996 July 09 and (b) 1997 July 10. Hatched zone is the location of the OAI based on the chemical profiles in Fig. 2. Letters on data points correspond to MB and MRP at that particular depth as determined by optical microscopy: c – coccoid MMB, sr – short-rod shaped MMB, lr – long-rod shaped GMB, mmp – many-celled magnetotactic prokaryote (GMB), p – magnetically responsive protist. Values of  $\delta_{FC}/\delta_{ZFC} > 2.0$  are characteristic of MMB and MRP that have magnetite magnetosomes organized in chains.

explain  $M_r/M_s < 0.5$  even within the OAI where SD magnetosomes were mostly concentrated. Based on the HTS values, there was more SPM material in the water column in and below the OAI in 1997 than there was in 1996 (Fig. 11), which may account for the lower values of  $M_r/M_s$  observed in 1997 (*cf.* Figs 5f and 6f).

## 4 DISCUSSION

### 4.1 Delta-delta ratios and the vertical distribution of magnetotactic bacteria

Delta-delta ratios  $> 2.0$  are characteristic of MB with magnetite magnetosomes organized in chains (Moskowitz *et al.* 1993; Carter-Stiglitz *et al.* 2002, 2004; Kopp *et al.* 2006a,b). It is unclear what the low-temperature magnetic response would be for magnetosomes

not aligned in simple linear chains within cells like those observed in the coccoid MMB and MRP (Figs 3a and 4). None has been measured in pure culture and may have delta-delta ratios less than 2. It is known that samples of extracted magnetosomes or lysed cells have  $\delta_{FC}/\delta_{ZFC} \approx 1$  (Moskowitz *et al.* 1993; Kopp *et al.* 2006a,b). Yet, within the OAI where the cocci MMB are dominant or in zones where MMB are absent but MRP are present in significant numbers, delta-delta ratios are still greater than 2.0 (Fig. 10). This observation suggests that, at least for these microorganisms, other types of magnetosome arrangements besides single linear chains produce delta-delta ratios above 2. Moreover, multiple chain arrangements observed in uncultured MMB from Lake Chiemsee also yield  $\delta_{FC}/\delta_{ZFC} > 2$  (Pan *et al.* 2005b). Both observations suggest that magnetosome arrangement plays a subordinate role to magnetosome composition in reducing  $\delta_{FC}/\delta_{ZFC}$  towards unity. Perhaps all

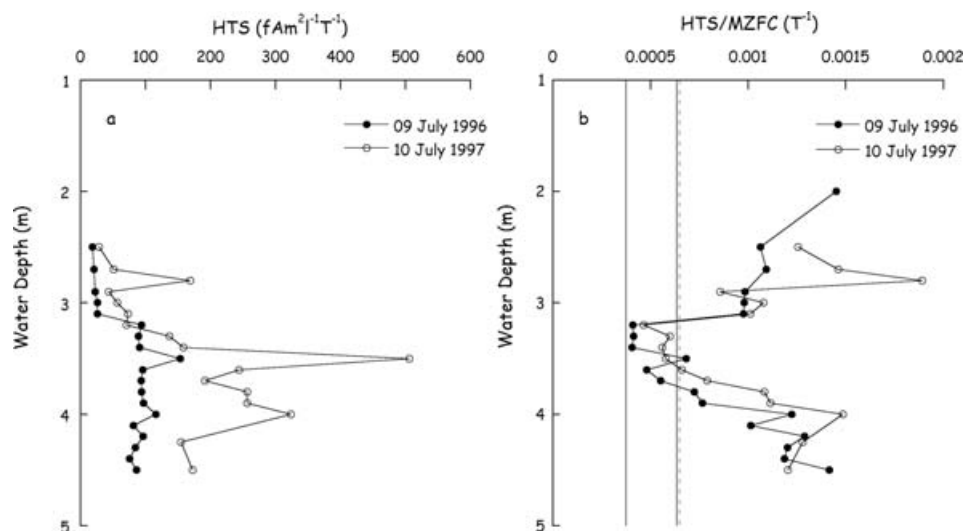


**Figure 11.** (a) HTS parameter as a function of water depth for data collected on 1996 July 09 and 1997 July 10. The HTS parameter is calculated from the slope of the ZFC/SIRM demagnetization curves between 120 and 220 K. (b) HTS/MZFC ratio as a function of water depth for data collected on 1996 July 09 and 1997 July 10. The two solid vertical lines represent the range of HTS/MZFC values for cultured MB (Moskowitz *et al.* 1993; unpublished data). The dash line represents a theoretical lower bound for HTS/MZFC (see text for details).

that is needed to produce  $\delta_{FC}/\delta_{ZFC} > 2$  is a consensus alignment of the long axes of magnetite crystals within MMB cells.

Unlike magnetite, greigite lacks a low-temperature remanence transition (Roberts 1995) and, therefore, greigite magnetosomes do not display marked changes in remanence below 300 K. Assuming a two component mixture of GMB ( $\delta_{FC}/\delta_{ZFC} \approx 1$ ) and MMB/MRP ( $\delta_{FC}/\delta_{ZFC} > 2.0$ ), delta ratios will vary between 1 and  $>2$  depending on the proportions of GMB and MMB/MRP (Moskowitz *et al.* 1993); therefore, the ratio can be used as a proxy for tracking the distribution of magnetite and greigite producers near and below the OAI. Finally, non-biogenic magnetite can also produce delta–delta values  $<2$ . However,  $\delta_{FC}/\delta_{ZFC}$  was less than 1.3 at shallow depths ( $<2.5$  m) in the oxic zone where no MB or MRP were found, and it will be assumed that this allochthonous non-biogenic magnetite (e.g. pedogenic, detrital, etc.) makes a negligible contribution in the water column.

#### 4.1.1 1996 profile

In 1996, just above the top of the OAI at 3.3 m, magnetization (ARM, SIRM,  $M_s$ , ZFC/SIRM, FCSIRM; Figs 5a and d) increases sharply between 3.1 and 3.2 m. This depth also corresponds to marked increases in  $M_r/M_s$  and  $\chi_{ARM}/SIRM$  indicating SD particles. At 3.1 m,  $\delta_{FC}/\delta_{ZFC}$  first becomes greater than 2.0, and at 3.2 m (Fig. 10a) microscopic observations show the first appearances of high densities of coccoid MMB and MRP. The largest delta–delta ratio occurs at the top of the OAI (3.2 m), where a short rod-shaped MMB first occurs in large numbers. Even at shallower depths ( $<3.1$  m), where the magnetization is low, the delta–delta ratio begins to steadily increase above the background signal ( $\delta_{FC}/\delta_{ZFC} \approx 1.3$ ) starting at 2.9 m, and at 3.0 m, where no MMB were observed, MRP were first detected. Passing through the OAI and just below it at 3.6 m, delta–delta ratios decrease with depth, but still maintain values  $>2.0$ . This zone also corresponds to the highest and nearly constant magnetization indicating fairly high and uniform abundances of MMB and MRP. It is unclear why the delta–delta ratio drops off with depth within the OAI. Possibly, the delta–delta ratio is strain specific related to the chain architecture [e.g. cocci (non-chain magnetosome arrangement) versus short rod (single magne-

tosome chain), MMB versus MRP], but there are few data on pure or enriched cultures to argue one way or the other (Moskowitz *et al.* 1993; Kopp *et al.* 2006a,b; Pan *et al.* 2005a,b). Another possibility is variable but slight oxidation ( $<1$  per cent) of magnetite magnetosomes, which can drive the delta–delta ratio to high or low values depending on the degree of non-stoichiometry (Moskowitz *et al.* 1993; Carter-Stiglitz *et al.* 2004). Whatever the reason, including experimental uncertainty, it is unlikely to be due to the presence of GMB because none were observed within the OAI or to an increase in SPM particles because the HTS/MZFC ratio is nearly constant within the OAI (Fig. 11).

The sharp drop in  $\delta_{FC}/\delta_{ZFC}$  to values  $<2.0$  at 3.7 m corresponds to the first occurrence of large numbers of the MMP and the long rod-shaped GMB. However, the delta–delta ratio does not drop to 1.0 as expected for 100 per cent greigite. The Verwey transition is still observed on the FCSIRM curves indicating that magnetite is still present and likely due to the short rod-shaped MMB and MRP, which were also observed at this depth. Interestingly, the delta–delta ratio increases again above 2.0 between 3.8 and 4.2 m (second peak at 3.9 m). This interval also corresponds to a zone where magnetization is steadily decreasing (Figs 5a and d) but  $\chi_{ARM}/SIRM$  remains above the SD value of  $2 \text{ mm A}^{-1}$  (Fig. 5e). These depth trends indicate that while the overall abundances of cells are decreasing with depth, MMB or MRP (either as living cells or as dead cells ‘raining down’ from the OAI) likely occur in sufficient numbers at these depths along with the GMB to drive the delta ratio back up above 2.0. No MMB were observed below 3.7 m, but cell inventories from 3.7, 3.8 and 4.2 m all show magnetic protists containing magnetite particles to be present.

#### 4.1.2 1997 profile

The 1997 results show that the zone of elevated delta–delta ratios is confined to the OAI, with a sharp increase at the top and a sharp drop at the bottom (Fig. 10b). The cell inventories show that at 3.4 m the short rod-shaped MMB is the dominant cell type along with several types of MRP. At the base of the OAI (3.5 m), several types of MRP dominate along with coccoid MMB and the first appearance of the MMP; however, at this depth  $\delta_{FC}/\delta_{ZFC}$  is still  $>2.0$

indicating that the MMP is present but in sufficiently low abundance compared to magnetite producers. This depth also corresponds to the highest values of ARM and SIRM (Figs 6a and b) and a spike in  $M_s$  (Fig. 6c). The delta–delta ratio dropped below 2.0 at 3.6 m where the MMP and Biflagellate ‘b’ MRP (Bazylnski *et al.* 2000) are the dominant organisms along with lesser amounts of coccooid MMB, large rod-shaped GMB and several other types of MRP.

As the delta–delta ratios continue to decrease with water depth below 3.5 m,  $M_s$  begins to increase again at 3.7 m until it spikes at its maximum value in the water column at 4.0 m (Fig. 6c). Within this zone of rising  $M_s$ , ARM and SIRM do not show corresponding increases and the cell inventory shows that the abundances of cells decrease with water depth. The spike in  $M_s$  is also not accompanied by a spike in FCSIRM or ZFCSIRM at 20K but rather a zone of nearly constant remanence. The SPM indicators (Fig. 11) show higher concentrations of SPM material and more of it relative to the SD fraction. Together these indicators suggest that the increase in  $M_s$  is not related to high abundances of MB or MRP but rather to an influx of SPM particles. At low temperatures both blocked SPM and SD magnetosome particles contribute to FCSIRM and ZFCSIRM but the SD fraction is decreasing with depth, whereas the SPM fraction is increasing with depth. These competing trends results in the observed break in slope in the FCSIRM and ZFCSIRM depth trends at the depth where  $M_s$  begins to increase (Figs 5d and 6d). An SPM component at these depths is also consistent with the  $\chi_{\text{ARM}}/\text{SIRM}$  ratios (Fig. 6e), which show an interval of near constant SD-like value below 3.8 m. Coarse grain PSD/MD particles ( $>0.1 \mu\text{m}$ ) or possible enhanced magnetostatic interactions within magnetosome arrangements that are not simple linear chains in MB and MRP cells should cause this ratio to decrease below the theoretical SD value (Egli & Lowrie 2002). By contrast, SPM particles should not affect this ratio at all because the ratio is entirely due to blocked SD particles. Without the ambiguity of PSD/MD or interacting SD contributions all the grain size indicators ( $M_r/M_s$ ,  $H_{\text{cr}}/H_c$ ,  $H_T$ ,  $H_c$ , see Figs 6e–h) can be interpreted as mixtures of SD and SPM particles with an increasing SPM component with depth below the OAI. Similar correlations are seen in the 1996 profile below 4.0 m between  $M_s$  and HTS/ARM,  $\chi_{\text{ARM}}/\text{SIRM}$  and the other grain size indicators (Figs 5 and 11) suggesting a similar but smaller increase in the SPM fraction at the bottom of the water column.

#### 4.2 Source of superparamagnetic material

The source of the SPM particles below the OAI is unclear as is their chemical composition (magnetite, greigite or some other Fe nanophase) but possible sources include: (1) reductive dissolution of the suspended detrital component (from above the OAI); (2) reductive dissolution of magnetite magnetosomes in dead MMB cells ‘raining down’ from shallower depths; (3) inorganic formation of nanophase particles of magnetite or greigite or (4) biologically induced iron mineralization by iron- or sulphate-reducing bacteria. Reductive dissolution of either the detrital component or the magnetite magnetosomes under high sulphide concentrations (up to 1 mM sulphide in 1997) below the OAI is highly unlikely as the main source of the SPM component for several reasons. First, the dissolution rate increases enormously with the inverse grain size, making the smallest SPM particles disappear almost instantaneously. In a system dominated by dissolution, the actual concentration of small particles is always extremely low. Secondly, since detrital particles in the water column are suspended for a relatively short time (approximately months), the amount of reductive dissolution would be minor (Canfield & Berner 1987; Hawthorne & McKenzie 1993; Egli

2004b). Finally, in 1997, there is actually a higher concentration of magnetic material below the OAI than present originally within or above the OAI, indicating there must be a new source of SPM particles at depth rather than just dissolution of the existing stock of magnetite magnetosomes or detrital magnetite. Nevertheless, some reductive dissolution of magnetite magnetosome chains may still occur below the OAI and account for the observed decrease in  $\chi_{\text{ARM}}/\text{SIRM}$  from its maximum values in the OAI (Figs 5e and 6e). Theory predicts the  $\chi_{\text{ARM}}/\text{SIRM}$  ratio is  $\propto d^2$  for non-interacting SD particles, where  $d$  is grain size, and partial dissolution of magnetosomes could cause the ARM ratio to decrease (Egli & Lowrie 2002; Egli 2004b). The ARM ratio was found to decrease by over an order of magnitude from its SD value in lake sediments from Baldeggersee (Switzerland) that were deposited under anoxic conditions (Egli 2004b) and for an anoxic sediment containing magnetofossils from Lake Baikal (Russia) (Egli 2004a; Chen *et al.* 2007). In both cases, probably the partial dissolution of magnetosome membranes, or the magnetite particles, or both can trigger chain collapse, which increases magnetostatic interactions and reduces the ARM (von Dobeneck *et al.* 1987; Egli 2004a,b; Kobayashi *et al.* 2006). While the ARM results from the anoxic zone in the water column in Salt Pond shows only about a 50 per cent reduction in  $\chi_{\text{ARM}}/\text{SIRM}$ , the observed drop in this ratio may be signalling the initial stages of magnetosome corrosion and chain collapse prior to deposition. A quantitative estimate of magnetite magnetosome preservation is given below.

Rather than reductive dissolution, a more likely explanation for the increasing SPM component with depth is authigenic formation of nanophase magnetic material either by abiotic or by BIM processes. For example, BIM greigite can form by biogeochemical interactions of iron with sulphide from bacterial sulphate reduction (Frankel & Bazylnski 2003). Greigite has been observed to form in association with the OAI in marine anoxic water columns of the Black Sea, Framvaren Fjord, Norway and Cariaco Basin, Venezuela (Cutter & Kluckholm 1999; Percy *et al.* 2007), which are larger, but chemically similar basins to Salt Pond. Dissimilatory iron-reducing bacteria, such as *Shewanella putrefaciens* can produce extracellular SPM magnetite under laboratory conditions (Bazylnski & Moskowitz 1997). Marine strains of these bacteria are known to be active at the OAI in the water columns of the Baltic and Black Seas (Nealson & Saffarini 1994). In addition, in laboratory experiments with *S. putrefaciens* CN32, extracellular magnetite particles have been observed to be sorbed to the cells (Glasauer *et al.* 2002), which would provide the mechanism for some fraction of the nanophase SPM particles to be retained on the 0.22- $\mu\text{m}$  filters used to process the Salt Pond water samples. However, because only magnetotactic microorganisms were assayed for at Salt Pond, we cannot substantiate directly the presence of dissimilatory iron-reducing bacteria in the water column at Salt Pond.

#### 4.3 MB and MRP abundances

Bulk saturation magnetization (Figs 5c and 6c) can be used to calculate the abundances of magnetite- and greigite-producing organisms using estimates of the dipole moments per cell based on average numbers of magnetosomes per cell, bulk magnetizations values of 480 kA m<sup>-1</sup> for magnetite and 125 kA m<sup>-1</sup> for greigite (Dunlop & Özdemir 1997) and identifying specific depths were either MMB or GMB separately exist. For magnetite producers like the coccooid MMB, the calculated dipole moment per cell is  $3.2 \times 10^{-15} \text{ Am}^2$  assuming a single chain of thirteen 80 nm diameter cubes of magnetite (Simmons *et al.* 2007). For greigite producers, the dipole

moment is calculated for the MMP found at Salt Pond, which consists of a 10–30 cell aggregate containing 491 magnetosomes, each with a diameter between 60–90 nm (Simmons *et al.* 2007). In this case, for an average particle size of 75 nm, the calculated dipole moment per MMP aggregate is  $2.59 \times 10^{-14}$  Am<sup>2</sup>. Finally, a baseline correction was applied to the  $M_s$  values by subtracting a mean value of  $M_s$  averaged over depths <2.5 m. This was necessary because  $M_s$  is a measure of contributions from all possible magnetic sources (biogenic, pedogenic, detrital and urban pollution). At water depths above 2.5 m, where no MMB or MRP were observed, the magnetization represents the non-biogenic allochthonous background.

During July 1996, at water depths between 3.2 and 3.5 m, magnetic producers are present (MMB and MRP) based on microscopic observations and high delta–delta ratios (Fig. 10a). In this interval, the coccoid MMB were found to be the most abundant. Within this zone, saturation magnetization (baseline corrected) is nearly constant with an average value of  $465 \text{ nA m}^2 \text{ l}^{-1}$  (Fig. 5c), yielding a MMB cell density of  $1.5 \times 10^5$  cells ml<sup>-1</sup>. At 3.7 m, where the MMP was first observed in high numbers and the delta–delta ratio sharply drops below 2 (Fig. 10a),  $M_s = 427 \text{ nA m}^2 \text{ l}^{-1}$ , yielding a MMP cell density of  $2 \times 10^4$  cells ml<sup>-1</sup>.

In 1997, the zone where magnetite producers are plentiful (microscopic observations and high delta–delta ratios; Fig. 10b) is in the OAI between 3.1 and 3.5 m. However, unlike the  $M_s$  trend in 1996,  $M_s$  (baseline corrected) steadily increases from  $168 \text{ nA m}^2 \text{ l}^{-1}$  at the top of OAI to  $2943 \text{ nA m}^2 \text{ l}^{-1}$  at the bottom (Fig. 6c), corresponding to MMB and MRP cell densities increasing from  $5 \times 10^4$  to  $9 \times 10^5$  ml<sup>-1</sup>. Although the MMP was observed along with other MMB at 3.5 m, it was not the dominant organisms at this depth. From microscopic observations, the MMP becomes dominant at 3.6 m (also, where delta–delta ratio drops below 2.0). At this depth,  $M_s = 1340 \text{ nA m}^2 \text{ l}^{-1}$  with a calculated MMP aggregate density of  $5 \times 10^4$  ml<sup>-1</sup>.

The magnetic results show that concentrations of the MMP were similar between 1996 and 1997 sampling dates, but the peak abundances of magnetite producers were approximately 10 times higher on 1997 July 10 compared to 1996 July 09. Furthermore, while the abundances of MMB and MRP were nearly constant within the OAI in 1996, they increased sharply by a factor of 10 or more from the top to the bottom of the OAI in 1997. In a recent study at Salt Pond, Simmons *et al.* (2004, 2007) and Simmons & Edwards (2006) using light microscopy and quantitative polymerase chain reaction (qPCR) assay found that the MMP occurred in their greatest number just below the OAI but never exceeded  $10^3$  ml<sup>-1</sup>. Similarly, the coccoid MMB reached cell densities of  $\approx 10^3$  ml<sup>-1</sup> at the top of the OAI in late 2004 June when the location of the OAI was similar to the 1996–1997 locations. Simmons *et al.* (2006) have also discovered two other MB at Salt Pond that show south-seeking behaviour, the opposite of typical MB found in the Northern Hemisphere. One, a chain of 2–5 cocci dubbed the ‘barbell’ whose magnetosome mineral composition is unknown, and the other, a small rod-shaped MMB, occurred in high numbers ( $10^4$ – $10^5$  ml<sup>-1</sup>) just below the OAI in association with the other MMB and GMB. Our estimated cell abundances based on the magnetization profiles yield cell densities for the coccoid MMB and MMP that are 10–100 times higher than abundances measured in 2004 by Simmons *et al.* (2004, 2007). Some of this difference can be attributed to the fact that magnetization measurements yield upper limits on the densities of the dominant organism and that both south-seeking organisms and the MRP contribute to the total magnetization. South-seeking MB would not have been detected during the 1996 and 1997 cell assays. Differences in cell abundances between sampling dates can

also come from sampling limitations. For example, sampling from discrete water depths on any given day may not be of sufficient resolution (time or position) to ‘catch’ thin layers of MB responding to changing geochemical conditions occurring on much finer scales. Still, it is likely that MB dynamics naturally fluctuate yearly and seasonally during summer stratification and changing geochemical conditions (Simmons *et al.* 2007).

#### 4.4 Iron concentrations

The saturation magnetization profile was integrated over the water column depth to obtain the total amount of Fe contained within suspended magnetic minerals. Two limits on this ‘magnetic’ Fe concentration was obtained by assuming the magnetization was entirely from either magnetite ( $M_s = 90 \text{ Am}^2 \text{ kg}^{-1}$ ) or greigite ( $M_s = 30 \text{ Am}^2 \text{ kg}^{-1}$ ; Dunlop & Özdemir 1997). The limits on the integrated Fe abundance in 1997 for the depth interval between 2.7 and 4.5 m was  $1.78 \times 10^{-5} \text{ kg-Fe m}^{-2}$  (as magnetite) or  $4.24 \times 10^{-5} \text{ kg-Fe m}^{-2}$  (as greigite). A similar calculation for the 1996 profile yielded limits of  $0.37 \times 10^{-5} \text{ kg-Fe m}^{-2}$  (as magnetite) to  $0.89 \times 10^{-5} \text{ kg-Fe m}^{-2}$  (as greigite) and shows that there was significantly less magnetic minerals suspended in the water column in 1996 than in 1997. In addition, the 1997 magnetic results can be compared to the total dissolved Fe(II) for the water column (depth interval 2.7–3.8 m) measured in Salt Pond on 1997 July 10 of  $89.7 \times 10^{-6} \text{ kg-Fe m}^{-2}$  (Fig. 2c). The magnetic iron minerals represent between 20.2 per cent (as magnetite) to 48.0 per cent (as greigite) of the total dissolved Fe(II). Because there was no Fe assay for water depths >3.8 m, it is uncertain if the peak in magnetization at 4.0 m (Fig. 6d) in 1997 also corresponded to an increase in dissolved Fe(II) at these depths. If so, then the calculated ‘magnetic’ Fe concentrations would be overestimated.

The magnetic mineral contribution to the Fe budget in the water column in 1997 can be further subdivided in a magnetite magnetosome component associated with the OAI and a magnetic mineral component associated with the sulphidic hypolimnion. Providing that all the Fe in the OAI was contained within magnetite magnetosomes, the integrated Fe abundances for the OAI depths in 1997 and 1996 were  $2.92 \times 10^{-6} \text{ kg-Fe m}^{-2}$  (1997, depth interval = 3.1–3.5 m) and  $0.90 \times 10^{-6} \text{ kg-Fe m}^{-2}$  (1996, depth interval 3.3–3.5 m). The magnetization measurements for 1997 indicate that  $\sim 3.3$  per cent of the total dissolved Fe(II) in the water column was sequestered in magnetite magnetosomes within the OAI.

Below the OAI where GMB and MMB coexist, it is more difficult to isolate the individual magnetic contributions from these two microorganisms, but again two limits on the ‘magnetic’ Fe concentration can be obtained assuming the magnetization is entirely from magnetite or greigite. In 1997, for the depth interval between 3.6 and 4.5 m, the limits are  $1.22 \times 10^{-5}$  and  $2.89 \times 10^{-5} \text{ kg-Fe m}^{-2}$  for magnetite and greigite, respectively. This corresponds to 13.6 per cent (as magnetite) to 32.2 per cent (as greigite) of the total dissolved Fe(II) in the whole water column and includes both Fe within magnetosomes and in other magnetite phases (e.g. BIM magnetic minerals). However, the magnetosome contribution should be even less here than within the OAI ( $\sim 3.3$  per cent) because of the much lower ARM (due to SD magnetosomes) below the OAI.

#### 4.5 Magnetofossil sediment flux and magnetosome preservation

Magnetosomes can be incorporated in sediment by two processes, depending on whether the OAI is located in the sediment or in the

overlying water column. In both cases, living MB will follow the OAI as its position changes with time, so that a permanent incorporation of magnetosomes occurs only for dead MB. If the OAI is located in the water column, as in Salt Pond, dead MB that are not incorporated into other organisms (e.g. grazing by protists) will sink to the sediment/water interface together with other material. The fraction of the total MB and MRP community that dies over a given time interval and escapes the OAI is not known. However, the magnetosome flux needed to explain typical magnetofossil concentrations in recent sediments with known sedimentation rates can be estimated. This concentration is typically orders of magnitude higher than the MB concentration in the water column. Therefore, can systems like Salt Pond produce sediments with high magnetofossil concentrations? To answer this question, the SIRM moment of all magnetosomes contained in a 1-m<sup>2</sup> water column ( $m_w$ ) can be compared with the SIRM moment of all magnetofossils contained in a 1-m<sup>2</sup> sediment deposited in 1 yr ( $f_s$ ).

The magnetosome SIRM in the water column can be estimated using the SIRM or the ARM profiles of Figs 5 and 6. The SIRM profiles are characterized by a detrital background that is clearly recognizable for depths above the OAI. Assuming that the total SIRM is given by the sum of a constant detrital background and a contribution from the magnetosomes, the magnetosome SIRM profile can be calculated by simply subtracting the background contribution. Similar to the calculation for Fe concentration, numerical integration over depth gives  $m_w$  of the entire water column, where  $m_w$  is expressed in m Am<sup>2</sup> (m<sup>2</sup> water column)<sup>-1</sup>. Alternatively, the ARM profile can also be used to estimate  $m_w$ . The ARM profiles show almost no background contribution, which is consistent with the fact that  $\chi_{\text{ARM}}/\text{SIRM}$  of the detrital magnetic particles is much lower than for the magnetosomes. Therefore, the ARM profile can be converted to magnetosome SIRM using  $\chi_{\text{ARM}}/\text{SIRM} \approx 3 \text{ mm A}^{-1}$  determined from the measurements within the OAI. This results in  $m_w \approx 0.22 \text{ mA m}^2 \text{ (m}^2 \text{ water column)}^{-1}$  for 1996 from either the ARM or the SIRM measurements, and  $m_w \approx 0.48\text{--}0.54 \text{ mA m}^2 \text{ (m}^2 \text{ water column)}^{-1}$  for 1997, where the lower value corresponds to the estimate obtained from the ARM.

Starting from the observed magnetization of dry sediment samples, the total magnetosome flux  $f_s$  can be calculated. Unfortunately, few data are presently available on the contribution of magnetofossils to the sediment magnetization and none is available from the sediments in Salt Pond. However, the SIRM of magnetofossils in some sediments has been estimated by Egli (2004a) using component analysis. SIRM values ranging from 0.6 to 1.5 mA m<sup>2</sup> (kg dry sediment)<sup>-1</sup> were measured for sediments of Lake Baldeggersee (Switzerland), Lake Geneva (Switzerland), and the Aral Sea (Uzbekistan/ Kazakstan), all of which did not experience significant reductive dissolution. The water content of the sediment samples from Baldeggersee was  $\approx 60$  per cent, with an annual varve thickness of 0.5 mm (Lotter & Birks 1997). Using a dry sediment density of 2700 kg m<sup>-3</sup>, a sedimentation rate of 1.35 kg (dry sediment) m<sup>-2</sup> is obtained. Using the magnetosome SIRM estimated from the sediment samples,  $f_s = 0.8\text{--}2 \text{ mA m}^2 \text{ (m}^2 \text{ sediment)}^{-1} \text{ yr}^{-1}$ .

Another example is given by Lake Ely (USA), where Kim *et al.* (2005) estimated a magnetofossil SIRM contribution of 50 per cent in the uppermost 10 cm of sediment using delta-delta ratios. This corresponds to a magnetosome SIRM of 4 mA m<sup>2</sup> kg<sup>-1</sup>. The sedimentation rate determined from sediment traps and from a freeze core was  $\approx 0.1 \text{ kg (m}^2 \text{ yr)}^{-1}$ . Using these data,  $f_s \approx 0.4 \text{ mA m}^2 \text{ (m}^2 \text{ sediment)}^{-1} \text{ yr}^{-1}$ .

The magnetosome flux  $f_s = 0.4\text{--}2 \text{ mA m}^2 \text{ (m}^2 \text{ sediment)}^{-1} \text{ yr}^{-1}$  obtained from the limited set of data described above can now be

compared with the water column  $m_w = 0.2\text{--}0.5 \text{ mA m}^2 \text{ (m}^2 \text{ water column)}^{-1}$  in Salt Pond. These estimates show that sediment deposited over one year contain 0.9–10 times (3 on average) the magnetosomes that are contained in the water column at a given time. This translates into a turnover time for magnetosomes of 1 month to 1 yr (4 months on average) if one assumes that MB exist during the entire year, or 0.5–6 months (2 months on average) if they exist only during summer stratification. The estimated turnover rates suggest that magnetosomes in the water column and in freshly deposited sediment are 2–6 months old. If the OAI results from Salt Pond are typical of other OAI systems, it is striking that, despite large differences in magnetization between sediment and water column (which suggests that MB living in the water column are not contributing significantly to the sediment magnetization), one needs just the total amount of MB living within the OAI (in order of magnitude) to produce the magnetofossil concentrations observed in some sediments.

While reductive dissolution of magnetite magnetosomes in the presence of sulphide was determined not to be the main source of SPM particles below the OAI, a certain amount of magnetite magnetosome dissolution is still expected to occur and affect the magnetosome sediment flux. Since sulphide is present below the OAI in Salt Pond to concentrations of 1 mM, it is possible that magnetite magnetosomes begin to dissolve while sinking in the water column. Canfield & Berner (1987) proposed the following rate law for dissolution of magnetite particles:

$$\frac{d}{dt} \log[\text{Fe}_3\text{O}_4] = -k[\text{S}^{2-}]A, \quad (1)$$

where  $[\text{Fe}_3\text{O}_4]$  is the amount of magnetite particles in arbitrary units,  $t$  is the time expressed in years,  $k$  is a reaction constant,  $[\text{S}^{2-}]$  is the sulphide concentration in mM, and  $A$  is the magnetite surface area in cm<sup>2</sup> g<sup>-1</sup>. Canfield & Berner (1987) obtained  $k \approx 1.1 \times 10^{-5}$  from laboratory experiments, while Canfield *et al.* (1992) estimated  $k \approx 2.2 \times 10^{-6}$  for magnetite crystals coated with pyrite. Both are consistent with direct estimates of  $k = (1.5\text{--}3.4) \times 10^{-6}$  for lake sediment magnetofossils undergoing reductive dissolution obtained by Egli (2004b). Using these data, together with  $A \approx 180 \times 10^3 \text{ cm}^2 \text{ g}^{-1}$  for typical magnetosome sizes and the sulphide concentrations reported in Fig. 2, the right-hand side of eq. (1) is  $\approx 0.4 \text{ yr}^{-1}$ . This can be used to estimate the amount of magnetite magnetosomes that survive dissolution along their typical water column lifetime  $T$  (most likely 2–6 months) given by the turnover rate. A lower bound for preserved biogenic magnetite is given by  $10^{-0.4T} = 60\text{--}90$  per cent, considering that magnetosomes will spend at least part of their lifetime  $T$  in the anoxic zone. Even higher magnetosome preservation potential is possible during settling if exposure to sulphidic conditions is further minimized by the surrounding cell membranes of dead MB. A certain but small degree of reductive dissolution of the magnetite magnetosomes is, therefore, expected below the OAI, which is supported by the observed decrease of  $\chi_{\text{ARM}}/\text{SIRM}$ . Although some of this drop in  $\chi_{\text{ARM}}/\text{SIRM}$  may also be related to magnetostatic interactions within non-chain magnetosome arrangements in 'unaltered' cells of MMB, MRP and GMB (Figs 3 and 4).

#### 4.6 Verwey transition temperatures

For both sampling dates, starting at the top of the OAI and extending down to the bottom of the sections, Verwey transition temperatures are nearly constant between 95 and 100 K. Similar Verwey transition temperatures (95–110 K) have been observed for several different strains of MMB grown in pure culture (Moskowitz *et al.* 1993;

Weiss *et al.* 2004; Kopp *et al.* 2006a; Pósfai *et al.* 2006a, Prozorov *et al.* 2007) and from enrichment cultures from Lake Chiemsee (Pan *et al.* 2005a,b). Freeze-dried cells of strain MV1 have on occasion been grown that give  $T_v \approx 115\text{--}117\text{ K}$  (Carter-Stiglitz *et al.* 2004; Prozorov *et al.* 2007) and upon laboratory aging (months to years)  $T_v$  decreases to about 100 K. These values are lower than the expected value of 120 K observed for ideal, stoichiometric magnetite (e.g. Dunlop & Özdemir 1997). It is known that very small amounts of non-stoichiometry (e.g. cation vacancies due to oxidation) can decrease the Verwey transition temperature while complete maghemitization ( $\text{Fe}_3\text{O}_4 \rightarrow \gamma\text{-Fe}_2\text{O}_3$ ) suppresses it entirely (Özdemir *et al.* 1993). This suggests that the magnetite magnetosomes in the MMB at Salt Pond are slightly non-stoichiometric; at least by the time the samples were measured in the laboratory (1–3 weeks after sampling). However, it is unclear if the non-stoichiometry is intrinsic to the magnetosome formation or a post-sampling or post mortem alteration effect. The fact that  $T_v \approx 100\text{ K}$  is observed for different strains of MMB processed by different sample preparation methods, for example, freeze-dried cells, whole-cell suspensions, enrichment samples, and filtered water samples, indicates it is independent of sampling handling and either represents (1) an intrinsic property of magnetite magnetosomes within living MMB or (2) a rapid post-mortem (bio)alteration of magnetosomes within dead cells (Pan *et al.* 2005b). Prozorov *et al.* (2007) suggest that reduced Verwey transition temperatures for MB is unrelated to non-stoichiometry and is an intrinsic effect related to thermal fluctuations in SD magnetosomes organized in chains.

The stoichiometry of magnetite magnetosomes is critical for the magnetite–maghemite battery hypothesis proposed by Vali & Kirschvink (1990) and Kopp (2007). According to this hypothesis, as MMB cycle back and forth across the OAI, magnetosomes are oxidized to maghemite above the OAI and reduced back to magnetite below the OAI, thereby liberating energy for metabolic activity. As Simmons & Edwards (2006) point out, for this to be an effective energy source, magnetosomes need to be oxidized fully to maghemite rather than a partially oxidized intermediary phase. Our results at Salt Pond do not readily support the magnetite–maghemite battery hypothesis because Verwey transition temperatures are independent of water depth and geochemical conditions associated with the OAI. This means that the chemical composition of the magnetite magnetosomes from MB remains approximately constant with depth, although the composition appears to be slightly non-stoichiometric magnetite. More importantly, pure maghemite would produce  $\delta_{\text{FC}}/\delta_{\text{ZFC}} \approx 1$  because it does not have a Verwey like remanence transition (Moskowitz *et al.* 1993; Özdemir *et al.* 1993). In Salt Pond, the highest delta–delta ratios occur within the OAI consistent with chains of magnetite magnetosomes rather than maghemite magnetosomes. It is possible that MB are cycling back and forth across the very top of the OAI at 3.1 m (1996) or 3.3 m (1997) rather within or at the bottom, but hardly any MB cells were observed, or any magnetic evidence for large contributions of SD (magnetosome) particles were detected, in the zone above the top of the OAI.

## 5 CONCLUSIONS

Chemically stratified aquatic environments, like Salt Pond, provide ideal type-sections to study magnetic, microbial and geochemical interactions. Profiles of magnetic properties across the OAI provide snapshots of the magnetic biomineralization that are not affected by eventual time-integrating and early diagenetic effects occurring in the sediment. Our main findings include the following.

1. At least four morphological types of MB, both magnetite and greigite producers, and several species of magnetically response protist are found associated with the OAI and the lower sulphidic hypolimnion. Sharp peaks in ARM and SIRM and SD-like values of  $\chi_{\text{ARM}}/\text{SIRM}$  occur within the OAI corresponding to high concentrations of MB and MRP with magnetically derived cell densities of  $10^4\text{--}10^6\text{ ml}^{-1}$ .

2. Low-temperature SIRM demagnetization curves show that magnetite is present in varying amounts throughout the water column, while delta–delta ratios clearly identified depths were chains of magnetite magnetosomes (in MMB or MRP) occur. The highest delta–delta ratios ( $>2.0$ ) marked the OAI where coccoid MMB were most abundant. Immediately below the bottom of the OAI, delta–delta ratios drop below 2.0 corresponding to the depth where the greigite-producing MMP first appear in high numbers. Surprisingly, in 1996, within the sulphidic hypolimnion, delta–delta ratios increase back above 2.0 indicating a zone where MMB or MRP occur in greater numbers than GMB.

3. The magnetization profile at Salt Pond reveals two important conclusions about MB contributions to the iron flux within the water column and their potential contribution to sediment magnetization. First, within the OAI, magnetic measurements in 1997 indicate that the amount of Fe sequestered in magnetite magnetosomes is no more than 3.3 per cent of the total available dissolved Fe(II) in the water column. This suggests that MMB are opportunistic in making use of a major iron source but have relatively little effect on it. Below the OAI in the sulphidic hypolimnion, magnetic minerals constitute a much larger fraction of the total dissolved Fe(II) ranging from 13.6 to 32.2 per cent depending on magnetic mineralogy. Magnetic measurements suggest that most of this iron is in the form of nanophase ( $<30\text{ nm}$ ) magnetic particles possibly associated with BIM processes occurring below the OAI. However, the composition of the BIM minerals could not be determined. Secondly, the OAI is a narrow but intense zone of SD particle production, and on an order of magnitude basis, you need just the total amount of MB living within an OAI to produce the magnetofossil concentrations observed in some sediment.

4. Verwey transition temperatures fell within a narrow range of values of 95–105 K and were observed to be independent of water depth and geochemical conditions. The values of  $T_v$  for MMB in Salt Pond are similar to those measured for individual strains of MMB grown in pure cultures, but reduced compared to  $T_v = 121\text{ K}$  for ideal, stoichiometric magnetite, indicative of minor amounts of non-stoichiometry. Reduced Verwey transition temperatures, therefore, appear to be an intrinsic property of magnetite magnetosomes whether grown in pure cultures or from a diverse population of MMB in the environment. This indicates that a limited amount oxygen non-stoichiometry ( $<1$  per cent) is present within magnetite magnetosomes, produced either initially during magnetosome formation or subsequently as an ‘aging’ process in living MMB. Therefore, reduced  $T_v$  values in biogenic SD magnetite in sediments do not necessarily indicate diagenetic alteration.

5. Finally, among the different magnetic properties defining the magnetic characteristics of Salt Pond, delta–delta ratios and  $\chi_{\text{ARM}}/\text{SIRM}$  are two magnetic proxies that best correspond to the geochemical signature of the OAI.

## ACKNOWLEDGMENTS

We thank B.L. Howes and D.R. Schlezinger for help in obtaining samples and chemical measurements, and M. Pósfai and B.

Carter-Stiglitz for discussions. The manuscript benefited from helpful comments by R. Kopp and an anonymous reviewer. This is IRM contribution 0704. The IRM is supported by the Instrumentation and Facilities programme, Earth Science Division, National Science Foundation. DAB is supported by US National Science Foundation grant EAR 0715492.

## REFERENCES

- Abreu, F., Martins, J.L., Silveira, T.S., Keim, C.N., Lins de Barros, H.G.P., Filho, F.J.G. & Lins, U., 2007. 'Candidatus Magnetoglobus multicellularis', a multicellular, magnetotactic prokaryote from a hypersaline environment, *Int. J. Syst. Evol. Microbiol.*, **57**, 1318–1322.
- Banerjee, S.K., 2006. Environmental magnetism of nanophase iron minerals: testing the biomineralization pathway, *Phys. Earth planet. Int.*, **154**, 210–221.
- Bazylinski, D.A. & Frankel, R.B., 2003. Biologically controlled mineralization in prokaryotes, in *Biomineralization*, Vol. 54: Reviews in Mineralogy, pp. 95–114, eds Weiner, S. & Dove, P.M., Mineralogical Society of America, Washington, DC.
- Bazylinski, D.A. & Moskowitz, B.M., 1997. Microbial biomineralization of magnetic iron minerals: microbiology, magnetism, and environmental significance, in *Geomicrobiology: Interactions Between Microbes and Minerals*, Vol. 35: Reviews in Mineralogy, pp. 181–224, eds Banfield, J.F. & Nealson, K.H., Mineralogical Society of America, Washington, DC.
- Bazylinski, D.A., Schlezinger, D.R., Howes, B.H., Frankel, R.B. & Epstein, S.S., 2000. Occurrence and distribution of diverse populations of magnetic protists in a chemically stratified coastal Salt Pond, *Chem. Geol.*, **169**, 319–328.
- Blakemore, R.P., 1975. Magnetotactic bacteria, *Science*, **190**, 377–379.
- Canfield, D.E. & Berner, R.A., 1987. Dissolution and pyritization of magnetite in anoxic marine sediments, *Geochim. Cosmochim. Acta*, **51**, 645–659.
- Canfield, D.E., Raiswell, R. & Bottrell, S., 1992. The reactivity of sedimentary iron minerals toward sulphide, *Am. J. Sci.*, **292**, 659–683.
- Carter-Stiglitz, B.S., Jackson, M. & Moskowitz, B.M., 2002. Low-temperature remanence in stable single-domain magnetite, *Geophys. Res. Lett.*, **29**, p. 1129, doi:10.1029/2001GL014197.
- Carter-Stiglitz, B.S., Moskowitz, B.M. & Jackson, M., 2004. More on the low-temperature magnetism of stable single domain magnetite: reversibility, and non-stoichiometry, *Geophys. Res. Lett.*, **31**, L06606, doi:10.1029/2003 GL019155.
- Chang, S.-B.R. & Kirschvink, J.L., 1989. Magnetofossils, the magnetization of sediments, and the evolution of magnetite biomineralization, *Ann. Rev. Earth Planet. Sci.*, **17**, 169–195.
- Chang, S.-B.R., Stolz, J.F., Kirschvink, J.L. & Awramik, S.M., 1989. Biogenic magnetite in stromatolites. II. Occurrence in ancient sedimentary environments, *Precambrian Res.*, **43**, 305–315.
- Chen, A., Egli, R. & Moskowitz, B.M., 2007. First-order reversal curve (FORC) diagrams of natural and cultured biogenic magnetic particles, *J. geophys. Res.*, **112**, B08S90, doi:10.1029/2006JB004575.
- Cline, J.D., 1969. Spectrophotometric determination of hydrogen sulfide in natural waters, *Limnol. Oceanogr.*, **14**, 454–458.
- Cutter, G.A. & Kluckhohn, R.S., 1999. The cycling of particulate carbon, nitrogen, sulfur, and sulfur species (iron monosulfide, greigite, pyrite, and organic sulfur) in the water columns of Framvaren Fjord and the Black Sea, *Mar. Chem.*, **67**, 149–160.
- Dunlop, D.J. & Özdemir, Ö., 1997. *Rock Magnetism: Fundamentals and Frontiers*, 573 pp., Cambridge University Press, Cambridge, UK.
- Egli, R., 2004a. Characterization of individual rock magnetic components by analysis of remanence curves, 1. Unmixing natural sediments, *Stud. Geophys. Geod.*, **48**, 391–446.
- Egli, R., 2004b. Characterization of individual rock magnetic components by analysis of remanence curves, 3. Bacterial magnetite and natural processes in lakes, *Phys. Chem. Earth*, **29**, 869–884.
- Egli, R. & Lowrie, W., 2002. Anhysteretic remanent magnetization of fine magnetic particles, *J. geophys. Res.*, **107**, 2209, doi:10.1029/2001JB000671.
- Fassbinder, J.W.E., Stanjek, H. & Vali, H., 1990. Occurrence of magnetic bacteria in soil, *Nature*, **343**, 161–163.
- Frankel, R.B., 1987. Anaerobes pumping iron, *Nature*, **330**, p. 208.
- Frankel, R.B. & Bazylinski, D.A., 2003. Biologically induced mineralization by bacteria, in *Biomineralization*, Vol. 54: Reviews in Mineralogy, pp. 217–247, eds Weiner, S. & Dove, P.M., Mineralogical Society of America, Washington, DC.
- Frankel, R.B., Bazylinski, D.A., Johnson, M.S. & Taylor, B.L., 1997. Magneto-aerotaxis in marine, coccoid bacteria, *Biophys. J.*, **73**, 994–1000.
- Gibbs-Eggar, Z., Jude, B., Dominik, J., Loizeau, J.L. & Oldfield, F., 1999. Possible evidence for dissimilatory bacterial magnetite dominating the magnetic properties of recent lake sediments, *Earth planet. Sci. Lett.*, **168**, 1–6.
- Giblin, A.E., 1990. *New England Salt Pond Data Book*, Technical Report WHOI-90-21, Woods Hole Oceanographic Institution.
- Glasauer, S., Langley, S. & Beveridge, T.J., 2002. Intracellular iron minerals in a dissimilatory iron-reducing bacterium, *Science*, **295**, 117–119.
- Hanzlik, M., Winklhofer, M. & Petersen, N., 2002. Pulsed-field-remnance measurements on individual magnetotactic bacteria, *J. Magn. Magn. Mater.*, **248**, 258–267.
- Hawthorne, T.B. & McKenzie, J.A., 1993. Biogenic magnetite: authigenesis and diagenesis with changing redox conditions in Lake Greifen, Switzerland, *SEPM Special Publ.*, **49**, 3–15.
- Hesse, P.P., 1994. Evidence for bacterial palaeoecological origin of mineral magnetic cycles in oxic and sub-oxic Tasman Sea sediments, *Mar. Geol.*, **117**, 1–17.
- Housen, B.A. & Moskowitz, B.M., 2006. Depth distribution of magnetofossils in near surface sediments from the Blake/Bahama Outer Ridge, western North Atlantic Ocean, determined by low-temperature magnetism, *J. geophys. Res.*, **111**, G04011, doi:10.1029/2005JG0000068.
- Kasama, T., Pósfai, M., Chong, R.K.K., Finlayson, A.P., Buseck, P.R., Frankel, R.B. & Dunin-Borkowski, R.E., 2006. Magnetic properties, microstructures, composition and morphology of greigite nanocrystals in magnetotactic bacteria from electron holography and tomography, *Am. Mineral.*, **91**, 1216–1229.
- Kim, B.Y., Kodama, K.P. & Moeller, R.E., 2005. Bacterial magnetite produced in water column dominates lake sediment mineral magnetism: Lake Ely, USA, *Geophys. J. Int.*, **163**, 26–37.
- Kobayashi, A., Kirschvink, J.L., Nash, C.Z., Kopp, R.E., Sauer, D.A., Bertani, L.E., Voorhout, F.W. & Taguchi, T., 2006. Experimental observation of magnetosome chain collapse in magnetotactic bacteria: sedimentological, paleomagnetic, and evolutionary implications, *Earth planet. Sci. Lett.*, **245**, 538–550.
- Komeili, A., Li, Z., Newman, D.K. & Jensen, G.J., 2006. Magnetosomes are cell membrane invaginations organized by the actin-like protein MamK, *Science*, **311**, 242–245.
- Kopp, R.E., 2007. The identification and interpretation of microbial biogeomagnetism, *PhD thesis*. California Institute of Technology, California.
- Kopp, R.E. & Kirschvink, J., 2008. The identification and biogeochemical interpretation of fossil magnetotactic bacteria, *Earth-Sci. Rev.*, **86**, 42–61.
- Kopp, R.E., Weiss, B.P., Maloof, A.C., Vali, H., Nash, C.Z. & Kirschvink, J.L., 2006a. Chains, clumps, and strings: magnetofossil taphonomy with ferromagnetic resonance spectroscopy, *Earth planet. Sci. Lett.*, **247**, 10–25.
- Kopp, R.E., Nash, C.Z., Kobayashi, A., Weiss, B.J., Bazylinski, D.A. & Kirschvink, J.L., 2006b. Ferromagnetic resonance spectroscopy for assessment of magnetic anisotropy and magnetostatic interactions: a case study of mutant magnetotactic bacteria, *J. geophys. Res.*, **111**, B12S25, doi:10.1029/2006JB004529.
- Leslie, B.W., Lund, S.P. & Hammond, D.E., 1990. Rock magnetic evidence for the dissolution and authigenic growth of magnetic minerals within anoxic marine sediments of the California continental borderland, *J. Geophys. Res. B: Solid Earth*, **95**, 4437–4452.

- Lotter, A.F. & Birks, H.J.B., 1997. The separation of the influence of nutrients and climate on the varve time-series of Baldeggersee, Switzerland, *Aquat. Sci.*, **59**, 362–275.
- Lovley, D.R. & Phillips, E.J.P., 1987. Rapid assay for microbially reducible ferric iron in aquatic sediments, *Appl. Environ. Microbiol.*, **52**, 751–757.
- McNeill, D.F., 1990. Biogenic magnetite from surface Holocene carbonate sediments, Great Bahama Bank, *J. geophys. Res. B: Solid Earth*, **95**, 4363–4372.
- Moskowitz, B.M., Frankel, R.B., Flanders, P.J., Blakemore, R.P. & Schwartz, B.B., 1988. Magnetic properties of magnetotactic bacteria, *J. Magn. Magn. Mater.*, **73**, 273–288.
- Moskowitz, B.M., Frankel, R.B., Bazylinski, D.A., Jannasch, H.W. & Lovley, D.R., 1989. A comparison of magnetite particles produced anaerobically by magnetotactic and dissimilatory iron-reducing bacteria, *Geophys. Res. Lett.*, **16**, 665–668.
- Moskowitz, B.M., Frankel, R.B. & Bazylinski, D.A., 1993. Rock magnetic criteria for the detection of biogenic magnetite, *Earth planet. Sci. Lett.*, **120**, 283–300.
- Muxworthy, A.R. & Williams, W., 2006. Low-temperature cooling behavior of single-domain magnetite: Forcing of the crystallographic axes and interactions, *J. geophys. Res.*, **111**, B07103, doi:10.1029/2006JB004298.
- Nealson, K. & Saffarini, D., 1994. Iron and manganese in anaerobic respiration: environmental significance, physiology, and regulation, *Annu. Rev. Microbiol.*, **48**, 311–343.
- Özdemir, Ö., Dunlop, D.J. & Moskowitz, B.M., 1993. The effect of oxidation of the Verwey transition in magnetite, *Geophys. Res. Lett.*, **20**, 1671–1674.
- Paasche, O., Lovlie, R., Dahl, S.O., Bakke J. & Nesje, A., 2004. Bacterial magnetite in lake sediments: late glacial to Holocene climate and sedimentary changes in northern Norway, *Earth planet. Sci. Lett.*, **223**, 319–333.
- Pan, Y., Petersen, N., Davila, A.F., Zhang, L., Winklhofer, M., Liu, Q., Hanzlik, M. & Zhu, R., 2005a. The detection of bacterial magnetite in recent sediments of Lake Chiemsee (southern Germany), *Earth planet. Sci. Lett.*, **232**, 109–123.
- Pan, Y., Petersen, N., Winklhofer, M., Davila, A.F., Liu, Q., Frederichs, T., Hanzlik, M. & Zhu, R., 2005b. Rock magnetic properties of uncultured magnetotactic bacteria, *Earth planet. Sci. Lett.*, **237**, 311–325.
- Peck, J.A. & King, J.W., 1996. Magnetofossils in the sediment of Lake Baikal, Siberia, *Earth planet. Sci. Lett.*, **140**, 159–172.
- Penninga, I., de Waard, H., Moskowitz, B.M., Bazylinski, D.A. & Frankel, R.B., 1995. Remanence measurements on individual magnetotactic bacteria using a pulsed magnetic field, *J. Magn. Magn. Mater.*, **149**, 279–286.
- Percy, D., Li, X., Taylor, G.T., Astor, Y. & Scranton, M.L., 2008. Controls on iron, manganese and intermediate oxidation state sulfur compounds in the Cariaco Basin, *Mar. Chem.*, in press.
- Petermann, H. & Bleil, U., 1993. Detection of live magnetotactic bacteria in South Atlantic deep-sea sediments, *Earth planet. Sci. Lett.*, **117**, 223–228.
- Petersen, N., von Dobeneck, T. & Vali, H., 1986. Fossil bacterial magnetite in deep-sea sediments from the South Atlantic Ocean, *Nature*, **320**, 611–615.
- Petersen, N., Weiss, D. & Vali, H., 1989. Magnetotactic bacteria in lake sediments, in *Geomagnetism and Paleomagnetism*, pp. 231–241, ed. F. Lowes, Kluwer Academic Publishers, Dordrecht.
- Pósfai, M., Moskowitz, B.M., Arató, B., Schüller, D., Flies, C., Bazylinski, D.A. & Frankel, R.B., 2006a. Properties of intracellular magnetite crystals produced by *Desulfovibrio magneticus* strain RS-1, *Earth planet. Sci. Lett.*, **249**, 444–455.
- Pósfai, M., Kasama, T. & Dunin-Borkowski, R.E., 2006b. Characterization of bacterial magnetic nanostructures using high-resolution transmission electron microscopy and off-axis electron holography, in *Magnetoception and Magnetosomes in Bacteria*, pp. 197–226, ed. D. Schüller, Springer-Verlag, Berlin.
- Prozorov, R., Prozorov, T., Mallapragada, S.K., Narasimhan, B., Williams, T.J. & Bazylinski, D.A., 2007. Magnetic irreversibility and Verwey transition in nano-crystalline bacterial magnetite, *Phys. Rev. B*, **76**, 054406, doi:10.1103/physRevB76.054406.
- Roberts, A.P., 1995. Magnetic properties of sedimentary greigite (Fe<sub>3</sub>S<sub>4</sub>), *Earth planet. Sci. Lett.*, **134**, 227–236.
- Scheffel, A., Gruska, M., Faivre, D., Linaroudis, A., Graumann, P., Plitzko, J.M. & Schüller, D., 2006. An acidic protein aligns magnetosomes along filamentous structure in magnetotactic bacteria, *Nature*, **440**, 110–114.
- Simmons, S.L. & Edwards, K.J., 2006. Geobiology of magnetotactic bacteria, in *Magnetoception and Magnetosomes in Bacteria*, pp. 77–102, ed. D. Schüller, Springer-Verlag, Berlin.
- Simmons, S.L., Sievert, S.M., Frankel, R.B., Bazylinski, D.A. & Edwards, K.J., 2004. Spatiotemporal distribution of marine magnetotactic bacteria in a seasonally stratified coastal Salt Pond, *Appl. Environ. Microbiol.*, **70**, 6230–6239.
- Simmons, S.L., Bazylinski, D.A. & Edwards, K.J., 2006. South seeking magnetotactic bacteria in the Northern Hemisphere, *Science*, **311**, 371–374.
- Simmons, S.L., Bazylinski, D.A. & Edwards, K.J., 2007. Population dynamics of marine magnetotactic bacteria in a meromictic Salt Pond described with qPCR, *Environ. Microbiol.*, **9**, 2162–2174.
- Smirnov, A.V. & Tarduno, J.A., 2000. Low-temperature magnetic properties of pelagic sediments (Ocean Drilling Program Site 805C): tracers of maghemitization and magnetic mineral reduction, *J. geophys. Res.*, **105**, 16 457–16 471.
- Snowball, I., Zillen, L. & Sandgren, P., 2002. Bacterial magnetite in Swedish varved lake sediments: a potential biomarker of environmental change, *Quatern. Int.*, **88**, 13–19.
- Tarduno, J.A., 1995. Superparamagnetism and reduction diagenesis in pelagic sediments: enhancement or depletion? *Geophys. Res. Lett.*, **22**, 1337–1340.
- Tauxe, L., Mullender, T.A.T. & Pick, T., 1996. Potbellies, wasp-waists, and superparamagnetism in magnetic hysteresis, *J. geophys. Res.*, **101**, 571–583.
- Thomas-Keppta, K.L. et al., 2000. Elongated prismatic magnetite crystals in ALH 84001 carbonate globules: potential Martian magnetofossils, *Geochim. Cosmochim. Acta*, **64**, 4049–4081.
- Torres de Araujo, F.F., Pires, M.A., Frankel, R.B. & Bicudo, C.E.M., 1985. Magnetite and magnetotaxis in algae, *Biophys. J.*, **50**, 375–378.
- Towe, K.M. & Moench, T.T., 1981. Electron-Optical Characterization of Bacterial Magnetite, *Earth planet. Sci. Lett.*, **52**, 213–220.
- Vali, H. & Kirschvink, J.L., 1990. Observations of magnetosome organization, surface structure, and iron biomineralization of undescribed magnetotactic bacteria: evolutionary speculations, in *Iron Biominerals*, pp. 97–115, eds Frankel, R.B. & Blakemore, R.P., Plenum Press, New York.
- Vali, H., von Dobeneck, T., Amarantidis, G., Förster, O., Morteani, G., Bachmann, L. & Petersen, N., 1989. Biogenic and lithogenic magnetic minerals in Atlantic and Pacific deep sea sediments and their paleomagnetic significance, *Geol. Rundsch.*, **78**, 753–764.
- von Dobeneck, T., Petersen, N. & Vali, H., 1987. Bakterielle Magnetofossilien – Paläomagnetische und paläontologische Spuren einer ungewöhnlichen Bakteriengruppe. *Geowiss. in unserer Zeit*, **5**, 27–35.
- Weiss, B.P., Kim, S.S., Kirschvink, J.L., Kopp, R.E., Sankaran, M., Kobayashi, A. & Komeili, A., 2004. Ferromagnetic resonance and low-temperature magnetic tests for biogenic magnetite, *Earth planet. Sci. Lett.*, **224**, 73–89.
- Yamazaki, T. & Kawahata, H., 1998. Organic carbon flux controls the morphology of magnetofossils in marine sediments, *Geology*, **26**, 1064–1066.